RESEARCH ARTICLE

Selective Inhibition of HDAC3 Targets Synthetic Vulnerabilities and Activates Immune Surveillance in Lymphoma

Patrizia Mondello[1], Saber Tadros[2], Matt Teater[1], Lorena Fontan[1], Aaron Y. Chang[3], Neeraj Jain[2], Haopeng Yang[2], Shailbala Singh[4], Hsia-Yuan Ying[1], Chi-Shuen Chu[5], Man Chun John Ma[2], Eneda Toska[6], Stefan Alig[7], Matthew Durant[1], Elisa de Stanchina[8], Sreejoyee Ghosh[2], Anja Mottok[9], Loretta Nastoupil[2], Sattva S. Neelapu[2], Oliver Weigert[7], Giorgio Inghirami[10], José Baselga[5], Anas Younes[11], Cassian Yee[4], Ahmet Dogan[12], David A. Scheinberg[3], Robert G. Roeder[5], Ari M. Melnick[1], and Michael R. Green[2,13,14]

ABSTRACT

CREBBP mutations are highly recurrent in B-cell lymphomas and either inactivate its histone acetyltransferase (HAT) domain or truncate the protein. Herein, we show that these two classes of mutations yield different degrees of disruption of the epigenome, with HAT mutations being more severe and associated with inferior clinical outcome. Genes perturbed by *CREBBP* mutation are direct targets of the BCL6–HDAC3 onco-repressor complex. Accordingly, we show that HDAC3-selective inhibitors reverse *CREBBP*-mutant aberrant epigenetic programming, resulting in: (i) growth inhibition of lymphoma cells through induction of BCL6 target genes such as *CDKN1A* and (ii) restoration of immune surveillance due to induction of BCL6-repressed IFN pathway and antigen-presenting genes. By reactivating these genes, exposure to HDAC3 inhibitors restored the ability of tumor-infiltrating lymphocytes to kill DLBCL cells in an MHC class I and II–dependent manner, and synergized with PD-L1 blockade in a syngeneic model *in vivo*. Hence, HDAC3 inhibition represents a novel mechanism-based immune epigenetic therapy for *CREBBP*-mutant lymphomas.

SIGNIFICANCE: We have leveraged the molecular characterization of different types of *CREBBP* mutations to define a rational approach for targeting these mutations through selective inhibition of HDAC3. This represents an attractive therapeutic avenue for targeting synthetic vulnerabilities in *CREBBP*-mutant cells in tandem with promoting antitumor immunity.

Downloaded from http://aacrjournals.org/cancerdiscovery/article-pdf/10/3/440/1813368/440.pdf by guest on 27 August 2022

[1]Division of Hematology/Oncology, Department of Medicine, Weill Cornell Medical College, New York, New York. [2]Department of Lymphoma & Myeloma, The University of Texas MD Anderson Cancer Center, Houston, Texas. [3]Molecular Pharmacology Program, Memorial Sloan Kettering Cancer Center, New York, New York. [4]Department of Melanoma Medical Oncology, The University of Texas MD Anderson Cancer Center, Houston, Texas. [5]Laboratory of Biochemistry and Molecular Biology, The Rockefeller University, New York, New York. [6]Department of Human Oncology and Pathogenesis, Memorial Sloan Kettering Cancer Center, New York, New York. [7]Department of Internal Medicine III, University Hospital of the Ludwig-Maximilians-University Munich, Munich, Germany. [8]Antitumor Assessment Core Facility, Memorial Sloan Kettering Cancer Center, New York, New York. [9]Institute of Pathology, University of Würzburg and Comprehensive Cancer Center Mainfranken, Würzburg, Germany. [10]Department of Pathology and Laboratory Medicine, Weill Cornell Medical College, New York, New York. [11]Department of Medicine, Memorial Sloan Kettering Cancer Center, New York, New York. [12]Department of Pathology and Laboratory Medicine, Memorial Sloan Kettering Cancer Center, New York, New York. [13]Department of Genomic Medicine, The University of Texas MD Anderson Cancer Center, Houston, Texas. [14]Center for Cancer Epigenetics, The University of Texas MD Anderson Cancer Center, Houston, Texas.

Note: Supplementary data for this article are available at Cancer Discovery Online (http://cancerdiscovery.aacrjournals.org/).

P. Mondello and S. Tadros contributed equally as co-first authors of this article. A.M. Melnick and M.R. Green contributed equally as co-senior authors of this article.

Corresponding Authors: Michael R. Green, The University of Texas MD Anderson Cancer Center, 1515 Holcombe Boulevard, Unit 903, Houston, TX 77030. Phone: 713-745-4244; E-mail: mgreen5@mdanderson.org; and Ari M. Melnick, Department of Medicine, Weill Cornell Medicine, 413 East 69th Street, New York, NY 10021. Phone: 646-962-6725; E-mail: amm2014@med.cornell.edu

Cancer Discov 2020;10:440–59

doi: 10.1158/2159-8290.CD-19-0116

©2020 American Association for Cancer Research.

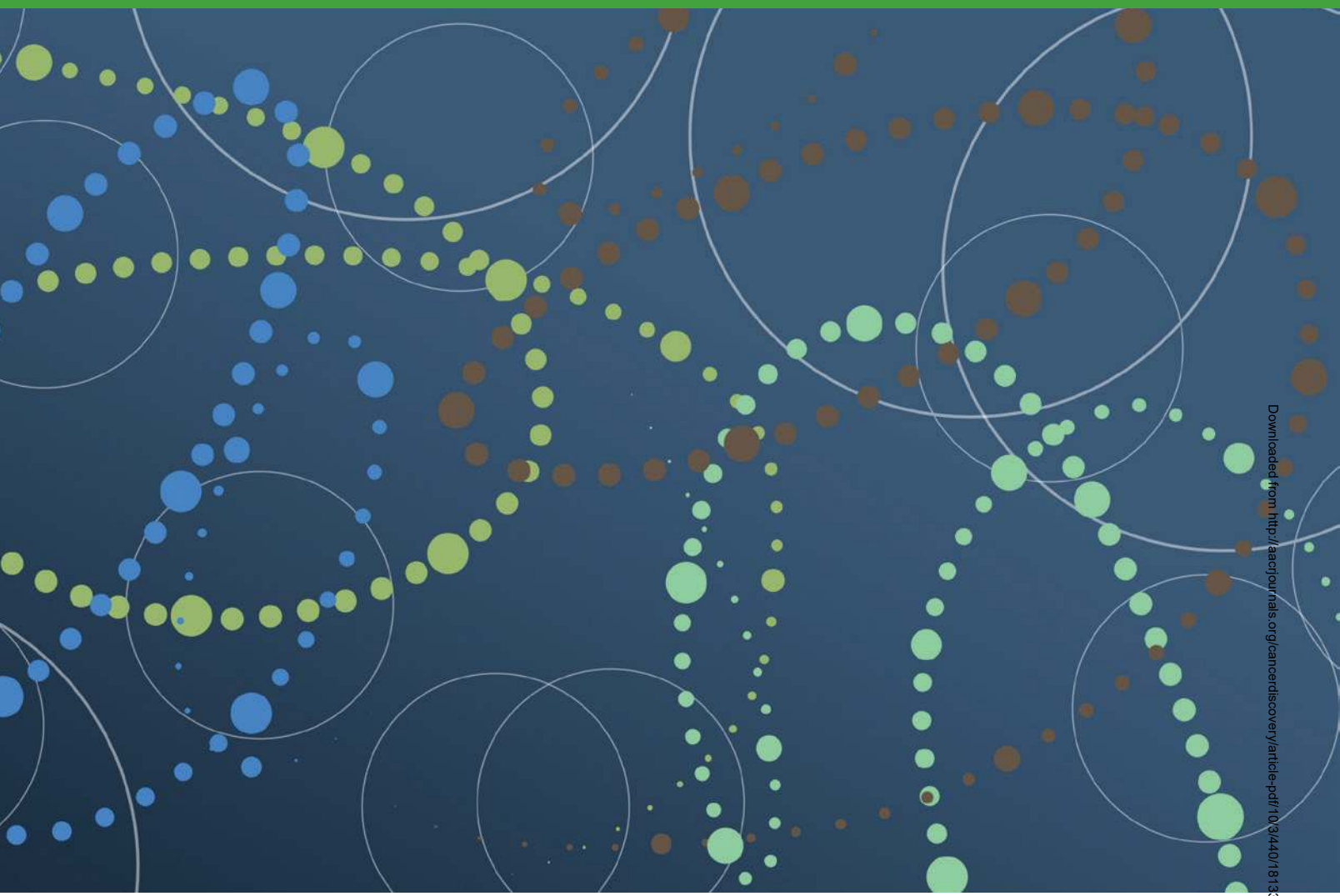

Downloaded from http://aacrjournals.org/cancerdiscovery/article-pdf/10/3/440/1813368/440.pdf by guest on 27 August 2022

INTRODUCTION

Diffuse large B-cell lymphoma (DLBCL) and follicular lymphoma are the two most frequent subtypes of non-Hodgkin lymphoma. These diseases originate from germinal center B (GCB) cells, which are at a stage of development that naturally allows for the proliferation and affinity maturation of antigen-experienced B cells to produce terminally differentiated memory B cells or plasma cells. The germinal center (GC) reaction is regulated by B cell–intrinsic activation and suppression of genes by master regulators such as the BCL6 transcription factor (1), and extrinsically via the interaction of GCB cells with follicular helper T (T_{FH}) cells and other immune cells within the GC (2). The BCL6 transcription factor is critical for GCB-cell development and coordinately suppresses the expression of large sets of genes by recruiting SMRT/NCOR corepressor complexes containing HDAC3 (3), the LSD1 histone demethylase (4), and tethering a noncanonical polycomb repressor 1–like complex in cooperation with EZH2 (5). These genes are normally reactivated to drive GC exit and terminal differentiation in the GC light zone, but the epigenetic control of these dynamically regulated GC transcriptional programs is perturbed in DLBCL and follicular lymphoma via the downstream effects of somatic mutation of chromatin-modifying genes (CMG; ref. 6).

The second most frequently mutated CMG in both DLBCL and follicular lymphoma is the *CREBBP* gene, which encodes a histone acetyltransferase that activates transcription via acetylation of histone H3 at lysine 27 (H3K27Ac) and other residues. We have previously found that these mutations arise as early events during the genomic evolution of follicular lymphoma and reside in a population of tumor-propagating cells, often referred to as common progenitor cells (CPC; ref. 7). We have also noted an association between *CREBBP* inactivation and reduced expression of MHC class II in human and murine lymphomas (7, 8). The expression of MHC class II is critical for the terminal differentiation of B cells through the GC reaction (9). The interaction with T helper cells via MHC class II results in B-cell costimulation through CD40 that drives NFκB activation and subsequent IRF4-driven suppression of BCL6. However, in B-cell lymphoma, tumor antigens may also be presented in MHC class II and recognized by $CD4^+$ T cells that drive an antitumor immune response (10, 11). The active suppression of MHC class II expression in B-cell

lymphoma may therefore be driven by evolutionary pressure against MHC class II–binding tumor antigens, as recognized in other cancers (12). In support of this notion, the reduced expression of MHC class II has been found to be associated with poor outcome in DLBCL (13, 14).

Recently, MHC class II expression has been defined as an important component of IFNγ-related signatures that are predictive of the activity of PD-1–neutralizing antibodies (14–17). This is consistent with a prominent role for $CD4^+$ T cells in directing antitumor immunity and responses to immunotherapy (18). Despite this, current immunotherapeutic strategies largely rely on the preexistence of an inflammatory microenvironment for therapeutic efficacy. Here, we have characterized the molecular consequences of *CREBBP* mutations and identified BCL6-regulated cell cycle, differentiation, and IFN signaling pathways as core features that are aberrantly silenced at the epigenetic and transcriptional level. We show that HDAC3 inhibition specifically restores these pathways, thus suppressing growth and most critically enabling T cells to recognize and kill lymphoma cells. Together, these findings highlight multiple mechanisms by which selective inhibition of HDAC3 can drive tumor-intrinsic killing as well as activate IFNγ signaling and antitumor immunity that extends to both *CREBBP* wild-type and *CREBBP*-mutant tumors.

RESULTS

CREBBP^{R1446C} Mutations Function in a Dominant Manner to Suppress BCL6 Coregulated Epigenetic and Transcriptional Programs

In B-cell lymphomas, the *CREBBP* gene is predominantly targeted by point mutations that result in single amino acid substitutions within the lysine acetyltransferase (KAT) domain (7, 19), with a hotspot at arginine 1446 (R1446) that leads to a catalytically inactive protein (20, 21). However, all of the prior studies characterizing the effects of *CREBBP* mutation have been performed using knockout (KO) or knockdown of *Crebbp*, resulting in loss of protein (LOP; refs. 8, 19, 22–25). Furthermore, mutations of R1446 have not been documented in any lymphoma cell line. We therefore opted to investigate whether there may be unique functional consequences of KAT domain hotspot mutations in *CREBBP*. To achieve this, we utilized CRISPR/Cas9-mediated gene editing with two unique guide RNAs (gRNA) to introduce the most common *CREBBP* mutation, R1446C, into a *CREBBP* wild-type cell line bearing the t(14;18)(q21;q32) translocation RL (Fig. 1A). This allowed us to generate clones from each gRNA that had received the constructs but remained wild-type (*CREBBP*^{WT}), those that edited their genomes to introduce the point mutations into both alleles (*CREBBP*^{R1446C}), and those that acquired homozygous frameshift mutations resulting in LOP (*CREBBP*^{KO}; Supplementary Fig. S1). These isogenic sets of clones differ only in their *CREBBP* mutation status, and therefore allow for detailed functional characterization in a highly controlled setting.

Western blot analysis confirmed that the CREBBP^{R1446C} protein was still expressed and that *CREBBP*^{KO} mutations resulted in a complete loss of protein expression (Fig. 1B). Western blotting with densitometry of the H3K27Ac mark revealed significant reduction in H3K27Ac in *CREBBP*^{R1446C} cells versus isogenic *CREBBP*^{WT} controls ($P < 0.001$; Fig. 1C). Although *CREBBP*^{KO} cells also showed lower H3K27Ac abundance than isogenic *CREBBP*^{WT} controls, this reduction was not statistically significant ($P = 0.106$). We performed chromatin immunoprecipitation sequencing (ChIP-seq) for H3K27Ac to define the physical location of these changes and identify potentially deregulated genes. This revealed 2,022 regions with significantly reduced acetylation, and 2,304 regions with significantly increased acetylation in *CREBBP*^{R1446C} cells compared with isogenic *CREBBP*^{WT} controls (fold change >1.5, q-value < 0.01; Fig. 1D; Supplementary Fig. S2; Supplementary Table S1). This pattern was mirrored by another CREBBP-catalyzed mark, H3K18Ac, and the loss or gain of histone acetylation was also accompanied by gain or loss of H3K27me3, respectively (Supplementary Fig. S3A–S3D). Regions with loss of H3K27Ac were observed to normally bear this mark in human GCB cells (ref. 24; Fig. 1D), suggesting that *CREBBP*^{R1446C} mutations lead to loss of a normal GCB epigenetic program. Notably, *CREBBP*^{KO} resulted in a reduction of H3K27Ac in these regions also, but at a lower magnitude than that observed with *CREBBP*^{R1446C} mutations (Fig. 1D and E). This was not observed for regions with increased H3K27Ac, which showed little change in *CREBBP*^{KO} cells.

Using RNA sequencing (RNA-seq), we observed broad changes in transcription, with 766 genes showing significantly increased expression and 733 genes showing significantly decreased expression in *CREBBP*^{R1446C} cells compared with *CREBBP*^{WT} isogenic controls (fold change >1.5, q-value < 0.01; Fig. 1F; Supplementary Table S2). The genes that were proximal to regions of H3K27Ac loss showed a coordinate reduction in transcript abundance and vice versa (FDR < 0.001; Fig. 1G), suggesting that these broad changes in transcription are directly linked to altered promoter/enhancer activity as a result of differential H3K27Ac. Importantly, we observed significant enrichment of the transcriptional signature induced by shRNA knockdown of *CREBBP* in murine B cells or human DLBCL cell lines (ref. 8; Fig. 1H). However, an even more significant enrichment was observed for the signature of genes we defined as being lost in association with *CREBBP* mutation in primary human *CREBBP* mutant follicular lymphoma B cells (ref. 7; FDR < 0.001; Fig. 1H). Consistent with our CRISPR cell line results, primary follicular lymphoma B cells with *CREBBP* LOP mutations were observed to have significantly less repression of this signature by single-sample gene set enrichment analysis (ssGSEA) compared with those with *CREBBP* KAT domain mutation ($P = 0.039$; Supplementary Fig. S4).

We used epigenetic and transcriptional profiles and hypergeometric analysis to gain insight into biological functions disrupted by *CREBBP*^{R1446C} mutations (Fig. 1I; Supplementary Tables S3 and S4). This confirmed a significant enrichment of genes downregulated in patients with *CREBBP*-mutant lymphoma, and further revealed an enrichment of BCL6–SMRT and BCL6 targets, consistent with the proposed role of CREBBP in opposing BCL6-mediated transcriptional repression. The biological functions of these genes included B-cell receptor (BCR) and NFκB signaling in addition to IFN signaling and antigen presentation (Fig. 1I). In line with the

Downloaded from http://aacrjournals.org/cancerdiscovery/article-pdf/10/3/440/1813368/440.pdf by guest on 27 August 2022

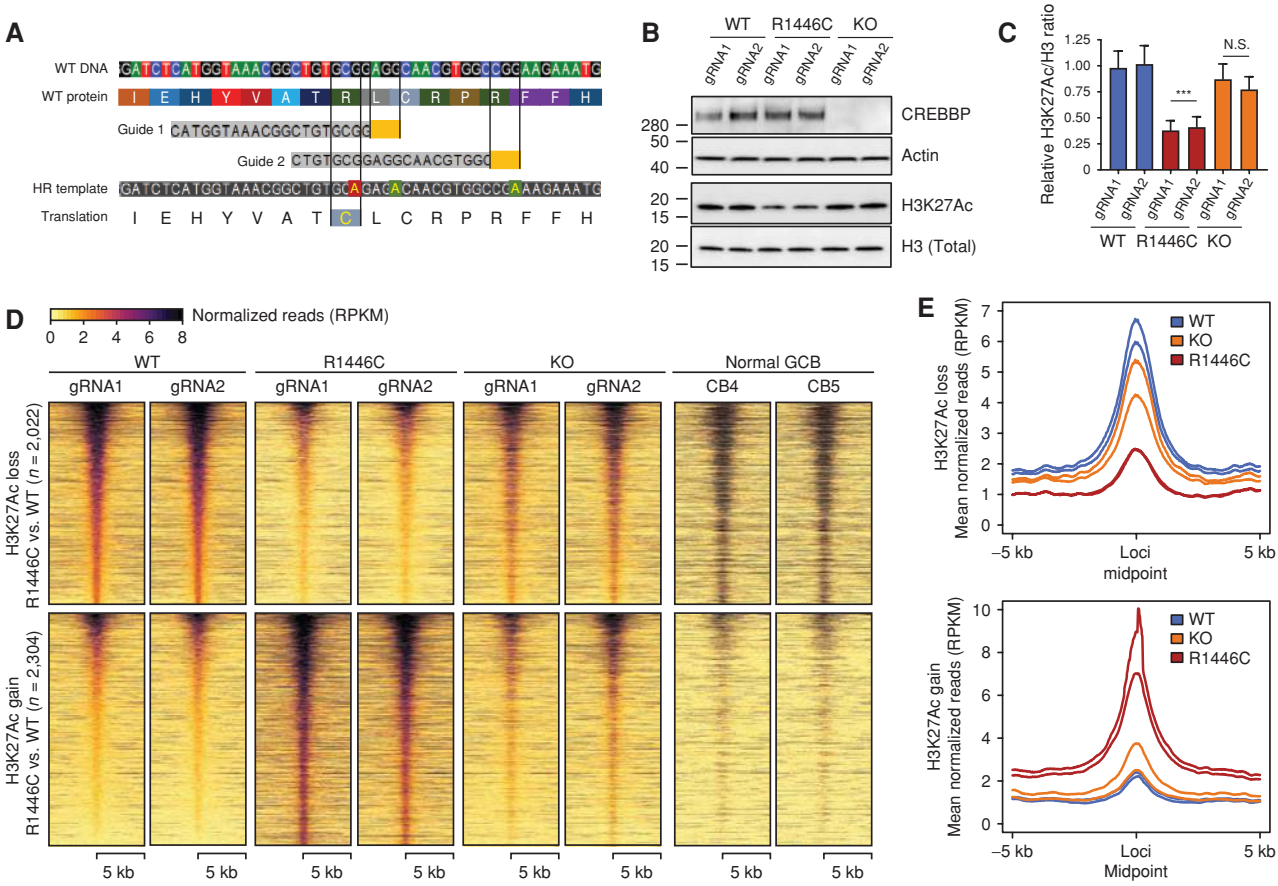

Figure 1. Detailed molecular characterization of *CREBBP*^{R1446C} and *CREBBP*^{KO} mutations using isogenic CRISPR/Cas9-modified lymphoma cells. **A,** A diagram shows the CRISPR/Cas9 gene-editing strategy. Two guides were designed that were proximal to the R1446 codon, with PAM sites highlighted in yellow. A single-stranded homologous recombination (HR) template was utilized that encoded silent single-nucleotide changes that interfered with the PAM sites but did not change the protein coding sequence, and an additional single-nucleotide change that encoded the R1446C mutation. **B,** A representative Western blot shows that the CREBBP^{R1446C} protein is expressed at similar levels to those of CREBBP^{WT}, whereas *CREBBP*^{KO} results in a complete loss of protein expression as expected. The level of H3K27Ac shows a more visible reduction in *CREBBP*^{R1446C} cells compared with isogenic *CREBBP*^{WT} cells than that observed in *CREBBP*^{KO} cells. **C,** Quantification of triplicate Western blot experiments shows that there is a significant reduction of H3K27Ac in *CREBBP*^{R1446C} cells compared with *CREBBP*^{WT} cells (*t* test, $P < 0.001$). A reduction is also observed in *CREBBP*^{KO} cells, but this was not statistically significant (*t* test, $P = 0.106$). **D,** Heat maps show the regions of significant H3K27Ac loss ($n = 2,022$, above) and gain ($n = 2,304$, below) in *CREBBP*^{R1446C} cells compared with isogenic WT controls. The regions with reduced H3K27Ac in *CREBBP*^{R1446C} cells can be seen to normally bear this mark in GCB cells. **E,** Density plots show that the degree of H3K27Ac loss (above) is most notable in *CREBBP*^{R1446C} cells compared with isogenic WT cells, whereas *CREBBP*^{KO} cells show an intermediate level of loss. Regions with H3K27Ac gain (below) in *CREBBP*^{R1446C} cells showed fewer changes in *CREBBP*^{KO} cells. (*continued on next page*)

enrichment of antigen-presenting pathways and the genome-wide differences in H3K27Ac patterning, we observed more severe reduction of H3K27Ac over the MHC class II locus in *CREBBP*^{R1446C} versus *CREBBP*^{KO} cells (Fig. 1J). This was associated with an approximately 2-fold reduction of cell surface MHC class II in *CREBBP*^{KO} cells compared with isogenic *CREBBP*^{WT} controls, but an approximately 37-fold reduction in *CREBBP*^{R1446C} cells (Fig. 1K). Notably, EP300 is expressed at a high level in all of the CRISPR-modified cell lines, and ChIP-qPCR showed that the MHC class II locus is bound by both CREBBP and EP300 in these cells (Supplementary Fig. S5A–S5C). Moreover, inhibition of EP300 activity in *CREBBP*^{KO} cells reduced the expression of MHC class II to levels similar to that in *CREBBP*^{R1446C} cells (Supplementary Fig. S5D), suggesting that the redundant activity of EP300 may partially sustain MHC class II expression in *CREBBP*^{KO} cells. These data further support a stronger epigenetic and transcriptional suppression of BCL6 target genes, including those involved in antigen presentation, with *CREBBP*^{R1446C} mutations compared with *CREBBP*^{KO}.

To confirm that the *CREBBP* KAT mutation is biologically active in primary GC B cells in a similar manner to that observed in CRISPR-engineered cell lines, we generated a novel genetically engineered mouse model with Cre-inducible expression of *Crebbp*^{R1447C} (equivalent to human R1446C). The endogenous *Crebbp* locus was engineered to switch from WT to mutant gene expression using a floxed inversion cassette (Supplementary Fig. S6A). These animals were crossed to mice engineered with the Cγ1-Cre allele to specifically induce recombination in GC B cells and bone marrow transplanted into irradiated CD45.1 recipients (Supplementary Fig. S6B and S6C). Transplanted mice were immunized with sheep

Downloaded from http://aacrjournals.org/cancerdiscovery/article-pdf/10/3/440/1813368/440.pdf by guest on 27 August 2022

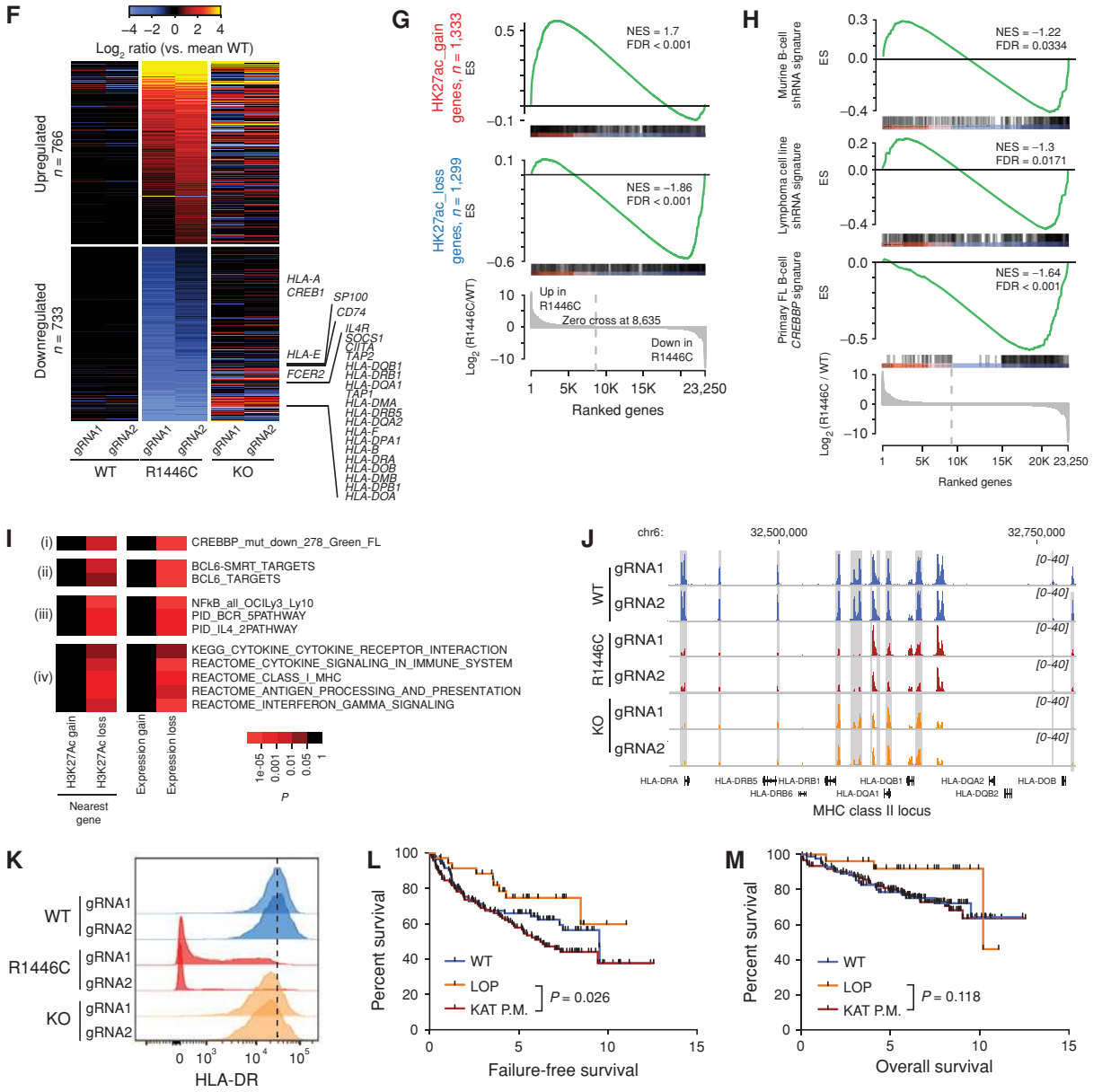

Figure 1. ***(Continued)*** **F,** A heat map of RNA-seq data shows that there are a similar number of genes with increased ($n = 766$) and decreased ($n = 733$) expression in *CREBBP*^{R1446C} cells compared with isogenic WT controls. The *CREBBP*^{KO} cells again show an intermediate level of change, with expression between that of *CREBBP*^{WT} and *CREBBP*^{R1446C} cells. **G,** Gene set enrichment analysis of the genes most closely associated with regions of H3K27Ac gain (above) or loss (below) shows that these epigenetic changes are significantly associated with coordinately increased or decreased expression in *CREBBP*^{R144C} cells compared with isogenic WT controls, respectively. **H,** Gene set enrichment analysis shows those genes that were previously found to be downregulated following shRNA-mediated knockdown of *CREBBP* in murine B cells (top) or human lymphoma cell lines (middle) are also reduced in *CREBBP*^{R1446C}-mutant cells compared with *CREBBP*^{WT} cells. However, the most significant enrichment was observed for the signature of genes that we found to be significantly reduced in primary human follicular lymphoma (FL) with *CREBBP* mutation compared with *CREBBP* WT tumors. **I,** Hypergeometric enrichment analysis identified sets of genes that were significantly overrepresented in those with altered H3K27Ac or expression in *CREBBP*^{R1446C} cells. This included (i) gene sets associated with *CREBBP* mutation in primary tumors, (ii) BCL6 target genes, (iii) BCR and IL4 signaling pathways, and (iv) gene sets involving immune responses; antigen presentation and IFN signaling were significantly enriched. **J,** ChIP-seq tracks of the MHC class II locus on chromosome 6 are shown for isogenic *CREBBP*^{WT} (blue), *CREBBP*^{R1446C} (red), and *CREBBP*^{KO} (orange) cells with regions of significant H3K27Ac loss shaded in gray. A significant reduction can be observed between *CREBBP*^{WT} and *CREBBP*^{R1446C} cells, with *CREBBP*^{KO} cells harboring an intermediate level H3K27Ac over these loci. **K,** Flow cytometry for HLA-DR shows that reduced H3K27Ac over the MHC class II region is associated with changes of cell-surface protein expression. An approximately 2-fold reduction is observed in *CREBBP*^{KO} cell compared with *CREBBP*^{WT}, but a dramatic, approximately 39-fold reduction is observed in *CREBBP*^{R1446C} cells. **L,** Kaplan–Meier plots show the failure-free survival in 231 previously untreated patients with follicular lymphoma according to their *CREBBP* mutation status. Nonsense/frameshift mutations that create a LOP are associated with a significantly better failure-free survival compared with KAT domain point mutations (KAT P.M.; log-rank $P = 0.026$). **M,** Kaplan–Meier plots show the overall survival in 231 previously untreated patients with follicular lymphoma according to their *CREBBP* mutation status. Patients with LOP mutations have a trend toward better overall survival, but this is not statistically significant (log-rank $P = 0.118$).

Downloaded from http://aacrjournals.org/cancerdiscovery/article-pdf/10/3/440/1813368/440.pdf by guest on 27 August 2022

red blood cells and sacrificed 10 days later when the GC reaction was at its peak (Supplementary Fig. S6C), whereupon flow cytometry was performed to assess B-cell populations. As expected, there was no perturbation of earlier stages of B-cell development (Supplementary Fig. S6D and S6E). Cre recombination was validated in sorted GC B cells (Supplementary Fig. S6F). *Cγ1Cre;Crebbp*$^{R1447C/+}$ GC B cells showed significantly reduced MHC class II expression compared with *Cγ1Cre;Crebbp*$^{+/+}$ controls ($P = 0.02$, Supplementary Fig. S6G), whereas (as expected) there was no difference in MHC II among naïve B cells from either genotype (Supplementary Fig. S6H). Finally, *Cγ1Cre;Crebbp*$^{R1447C/+}$ mice manifested a significantly skewed light-zone:dark-zone ratio in favor of increased dark-zone cells ($P = 0.01$; Supplementary Fig. S6I–S6L), which are the cells that most reflect the actions of BCL6, although the overall abundance of GC B cells was not increased (Supplementary Fig. S6M and S6N). These results confirm in primary cells our MHC class II findings from CRISPR/Cas9-edited clones and hence their value as a platform for mechanistic studies.

Finally, mutations in *CREBBP* have been previously associated with adverse outcome in follicular lymphoma and are incorporated into the M7-FLIPI prognostic index (26). However, in these analyses, all *CREBBP* mutations were considered collectively without discriminating between KAT domain point mutations and nonsense/frameshift LOP mutations. We therefore reevaluated these data in light of our observed functional differences between these mutations. This showed that there was a significant difference in failure-free survival (Fig. 1L) between patients with these two classes of *CREBBP* mutations. This was not significant for overall survival (Fig. 1M). Specifically, patients bearing KAT domain point mutations in *CREBBP* (22% of which were R1446 mutations) had a significantly reduced failure-free survival compared with patients with LOP mutations in *CREBBP* (log-rank $P = 0.026$), with no other clinical factors being significantly different between these groups (Supplementary Table S5). Collectively, these results provide the first direct experimental description of the role of *CREBBP*^{R1446C} mutations in lymphoma B cells. Our data suggest that *CREBBP* KAT domain mutations may have a potential dominant repressive function on loci that can be targeted by redundant acetyltransferases, thereby driving a more profound molecular phenotype that is associated with a worse patient outcome.

Synthetic Dependence on HDAC3 in *CREBBP*-Mutant DLBCL Is Independent of Mutation Subtype

Our genomic analysis showed that BCL6 target genes were significantly enriched among those with reduced H3K27Ac and gene expression in *CREBBP*^{R1446C} cells. We therefore evaluated CREBBP and BCL6 binding over these regions using data from normal GC B cells (24) and found that the regions with *CREBBP*^{R1446C} mutation–associated H3K27Ac loss are bound by both proteins at significantly higher levels than H3K27Ac peaks that remain unchanged with *CREBBP* mutation (CREBBP Wilcoxon $P = 1.2^{-41}$; BCL6 Wilcoxon $P = 2.83^{-52}$) or peaks with increased H3K27Ac in *CREBBP*^{R1446C} mutants (CREBBP Wilcoxon $P = 3.01^{-137}$; BCL6 Wilcoxon $P = 3.17^{-128}$; Fig. 2A). This suggests that these genes may be antagonistically regulated by CREBBP and BCL6, the latter of which mediates gene repression via recruitment of HDAC3-containing NCOR/SMRT complexes (3, 27). The epigenetic suppression of gene expression in *CREBBP*-mutant cells may therefore be dependent upon HDAC3-mediated suppression of BCL6 target genes. Using a selective HDAC3 inhibitor, BRD3308 (28), we found that *CREBBP*^{R1446C} and *CREBBP*^{KO} clones showed greater sensitivity to HDAC3 inhibition compared with isogenic WT controls in cell-proliferation assays (Fig. 2B). We confirmed this as being an on-target effect of BRD3308 by performing shRNA knockdown of *HDAC3* and observing a greater effect on cell proliferation in *CREBBP*^{R1446C} cells compared with isogenic controls (Fig. 2C; Supplementary Fig. S7). Moreover, HDAC3 inhibition was able to efficiently promote the accumulation of H3K27Ac in a dose-dependent manner in both *CREBBP*^{WT} and *CREBBP*^{R1446C} cells, as compared with the inactive chemical control compound BRD4097 (Fig. 2D). This suggests that the increased sensitivity to HDAC3 inhibition in *CREBBP*^{R1446C} cells may be linked with an acquired addiction to an epigenetic change driven by *CREBBP* mutation. We posited that one of these effects may be the suppression of *CDKN1A* (encoding p21) expression, which is a key BCL6 target gene (29) that has reduced levels of H3K27Ac in both *CREBBP*^{R1446C} and *CREBBP*^{KO} cells (Fig. 2E). In support of this, we observed a marked induction of p21 expression by BRD3308 (Fig. 2F) and observed that shRNA-mediated silencing of *CDKN1A* partially rescued the effect of BRD3308 on cell proliferation (Fig. 2G). Therefore, *CREBBP* mutations, regardless of type, sensitize cells to the effects of HDAC3 inhibition in part via the induction of p21.

We aimed to confirm this trend using a larger panel of DLBCL cell lines with either WT ($n = 6$) or mutant *CREBBP* ($n = 6$). This revealed a significantly lower effective dose 50 (ED_{50}) of BRD3308 in *CREBBP* mutant compared with WT cell lines ($P = 0.002$, Fig. 2H–I). We did not observe this trend using the nonspecific HDAC inhibitors romidepsin and SAHA (Supplementary Fig. S8). Notably, none of these cell lines harbor KAT domain missense mutations in *CREBBP*, providing further evidence that sensitivity to HDAC3 selective inhibition is independent of mutation type (i.e., KAT domain missense vs. nonsense/frameshift). Furthermore, we also observed the induction of p21 expression and apoptosis in *CREBBP* WT cell lines, although to a lesser degree (Supplementary Fig. S9). To gain greater insight into this, we performed RNA-seq of *CREBBP* WT (OCI-Ly1) and *CREBBP*-mutant (OCI-Ly19, OZ) cell lines treated with BRD3308. Notably, the ability of HDAC3 inhibition to induce the expression of genes involved in the terminal differentiation of B cells was conserved in both WT and mutant cell lines (Fig. 2J). These results are consistent with the role of BCL6 in controlling checkpoints, terminal differentiation, and other functions (1) and point toward induction of these transcriptional programs as contributing to the antilymphoma response induced by HDAC3 inhibition in both the *CREBBP* WT and *CREBBP*-mutant settings. Although targetable by HDAC3 inhibition in WT cells, the BCL6–HDAC3 target gene set is more significantly perturbed in the context of *CREBBP* mutation leading to an enhanced cell-intrinsic effect of HDAC3 inhibition.

Downloaded from http://aacrjournals.org/cancerdiscovery/article-pdf/10/3/440/1813368/440.pdf by guest on 27 August 2022

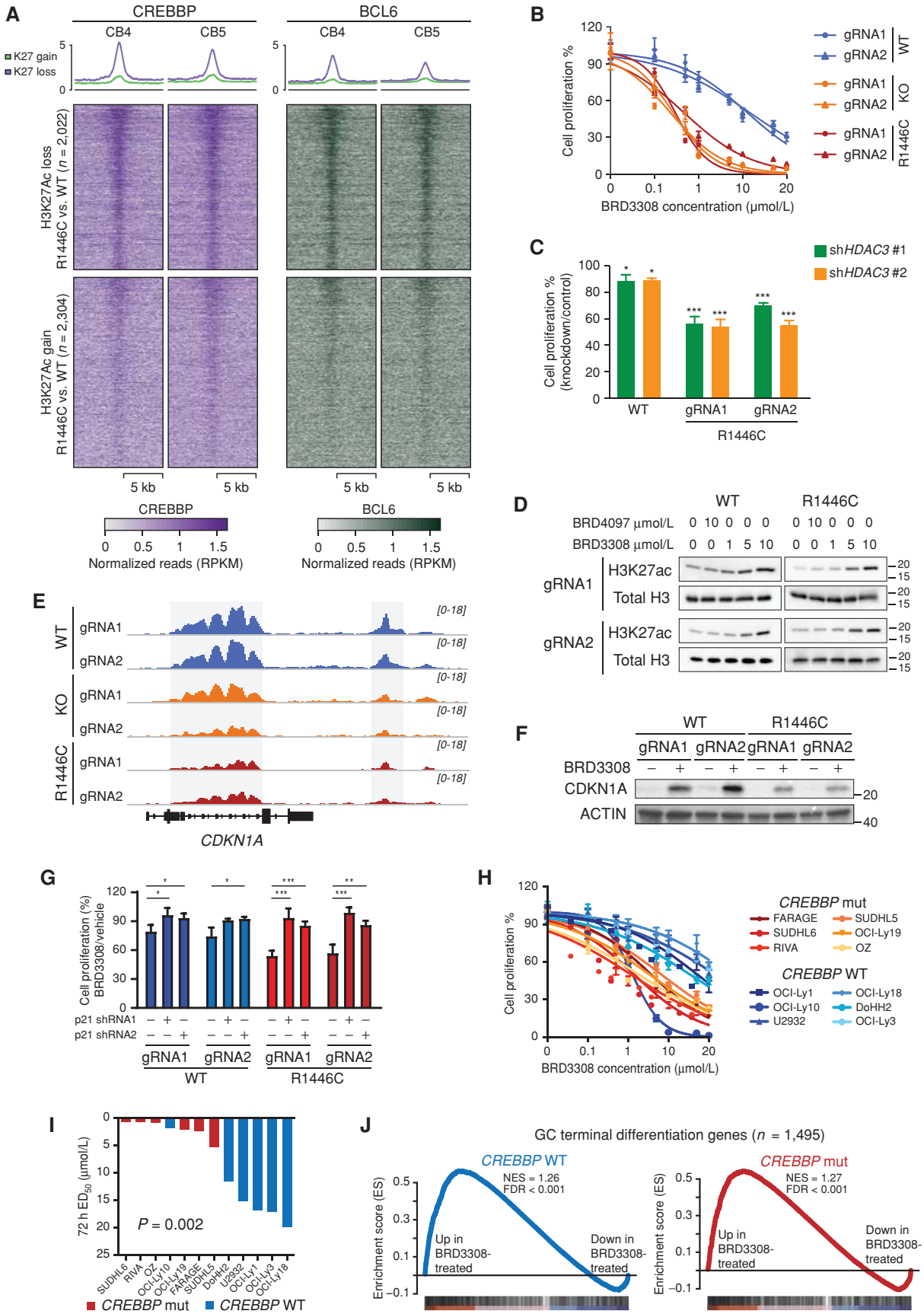

Downloaded from http://aacrjournals.org/cancerdiscovery/article-pdf/10/3/440/1813368/440.pdf by guest on 27 August 2022

HDAC3 Inhibition Is Active against Primary Human DLBCL

Our observation that HDAC3 inhibition can affect both *CREBBP* mutant and WT B cells led us to test its efficacy in primary patient-derived xenograft (PDX) models of DLBCL. To achieve this, we first expanded *CREBBP* WT tumors *in vivo* and transitioned them to our novel *in vitro* organoid system for exposure to BRD3308 (30). All tumors that were tested showed a dose-dependent reduction in cell viability when cultured with BRD3308, compared with the vehicle control (Fig. 3A). We therefore treated 3 of these *CREBBP* WT tumors *in vivo* with either 25 mg/kg or 50 mg/kg of BRD3308, which led to a significant reduction in growth of PDX tumors treated with either dose compared with vehicle control (Fig. 3B). We were able to obtain only a single primary human *CREBBP*-mutant (R1446C) DLBCL PDX model, which could be grown only by renal capsule implantation. Treatment of these tumors with 25 mg/kg BRD3308 and monitoring by weekly MRI (Fig. 3C) showed a significant reduction in growth compared with vehicle control–treated tumors (Fig. 3D). In line with our cell line models, quantitative PCR analysis of treated PDX tumors showed an induction of BCL6 target genes with a role in B-cell terminal differentiation, including *IRF4, PRDM1, CD138*, and *CD40* compared with vehicle-treated tumors (Supplementary Fig. S10). Therefore, selective inhibition of HDAC3 may be a rational approach for targeting the aberrant epigenetic silencing of BCL6 target genes in primary human B-cell lymphoma.

Selective Inhibition of HDAC3 Reverts the Molecular Phenotype of *CREBBP* Mutations

We aimed to take a deeper look at the molecular consequences of HDAC3 inhibition by performing H3K27Ac ChIP-seq and RNA-seq of *CREBBP*^{R1446C}-mutant cells after exposure to BRD3308, as compared with the inactive negative control compound BRD4097. This showed that selective HDAC3 inhibition promoted the gain of H3K27Ac over a broad number of regions ($n = 6{,}756$; Fig. 4A). Strikingly, HDAC3 inhibition significantly either restored or further increased the abundance of H3K27Ac at 28% (558/1,975) of sites that became deacetylated in *CREBBP*^{R1446C} (hypergeometric enrichment $P = 3.02^{-178}$), consistent with the role of HDAC3 in opposing CREBBP functions (Fig. 4B). Indeed, a more quantitative analysis indicated HDAC3 inhibition coordinately increased the level of H3K27Ac over the same loci that showed reduced levels in *CREBBP*^{R1446C} compared with *CREBBP*^{WT} cells, although this restoration of H3K27Ac was not sufficient to completely revert the epigenomes of *CREBBP*^{R1446C} cells to the level that was observed in *CREBBP*^{WT} cells (Fig. 4C). In line with the role of HDAC3 and BCL6 in transcriptional repression, BRD3308 induced an expression profile that was markedly skewed toward gene upregulation ($n = 1{,}467$ vs. 208 genes downregulated; Fig. 4D; Supplementary Table S6 and S7), including upregulation of IFN-responsive genes such as antigen-presenting machinery and PD-L1 (*CD274*). Notably, the genes with increased expression following HDAC3 inhibition were significantly enriched for those that lose H3K27Ac in *CREBBP*^{R1446C}-mutant compared with WT (FDR < 0.001; Fig. 4E), further supporting the conclusion that HDAC3 inhibition directly counteracts changes associated with *CREBBP* mutation. A quantitative assessment of ChIP-seq signal indicated that enhancers manifested greater gain of H3K27Ac as compared with promoters in cells exposed to HDAC3i (Wilcoxon $P < 0.001$; Fig. 4F), although MHC class II genes also showed coordinate increases in promoter H3K27Ac (Fig. 4G). Analysis of critical gene loci that are deregulated by *CREBBP* mutation, such as the MHC class II gene cluster and *CIITA*, exemplify this induction of H3K27ac (Fig. 4H–I). We validated the increased H3K27Ac and expression of these genes in independent experiments wherein *CREBBP*^{R1446C} or isogenic control cells were treated with BRD3308 or vehicle, H3K27Ac was measured by ChIP-qPCR (Supplementary Fig. S11), and transcript abundance was measured by qPCR ($P < 0.001$; Fig. 4J). We further validated that this was an on-target effect of BRD3308 by performing shRNA-mediated knockdown of *HDAC3*, which resulted in the increased expression of these genes relative to control shRNA (Fig. 4K). Together, these data indicate that the aberrant mutant *CREBBP* epigenetic and transcriptional program can be restored by selective pharmacologic inhibition of HDAC3.

HDAC3 Inhibition Counteracts BCL6 Target Gene Repression in Lymphoma Cells Including IFN Response, Irrespective of *CREBBP* Mutation Status

IFN signaling and antigen-presenting genes have not been well investigated as downstream targets of BCL6–HDAC3

Downloaded from http://aacrjournals.org/cancerdiscovery/article-pdf/10/3/440/1813368/440.pdf by guest on 27 August 2022

Figure 2. Synthetic dependence upon BCL6 and HDAC3 in *CREBBP*-mutant cells. **A,** A heat map shows that regions with reduced H3K27Ac in *CREBBP*^{R1446C} cells compared with *CREBBP*^{WT} cells (above) are bound by both CREBBP and BCL6 in normal germinal center B cells. This binding is not observed over regions with increased H3K27Ac in mutant cells. **B,** Isogenic *CREBBP*^{R1446C} and *CREBBP*^{KO} cells have a greater sensitivity to BRD3308, a selective HDAC3 inhibitor, compared with *CREBBP*^{WT} cells. **C,** Knockdown of *HDAC3* with two unique shRNAs shows a similar preference toward limiting cell proliferation in *CREBBP*^{R1446C} cells compared with WT. Data are shown relative to control shRNA in the same cell lines (*, $P < 0.05$; ***, $P < 0.001$). **D,** Representative Western blots show a dose-dependent increase in H3K27Ac in both *CREBBP*^{WT} and *CREBBP*^{R1446C} cells treated with BRD3308, compared with the control compound BRD4097. **E,** ChIP-seq tracks of H3K27Ac show that *CREBBP*^{KO} and *CREBBP*^{R1446C} both have reduced levels over the *CDKN1A* locus compared with isogenic *CREBBP*^{WT} cells. Regions that are statistically significant are shaded in gray. **F,** A representative Western blot shows that CDKN1A is induced at the protein level by treatment with 10 μmol/L BRD3308 in both *CREBBP*^{WT} and *CREBBP*^{R1446C} cells. **G,** Knockdown of *CDKN1A* (p21) using two unique shRNAs partially rescued the proliferative arrest of cells treated with BRD3308. This rescue was more significant in *CREBBP*-mutant cells compared with WT. Data are displayed relative to vehicle-treated cells (*, $P < 0.05$; **, $P < 0.01$; ***, $P < 0.001$). **H,** The difference in sensitivity to BRD3308 between *CREBBP* WT (blue) and *CREBBP* mutant (yellow to red) was validated in a large panel of DLBCL cell lines. **I,** The ED_{50} concentrations for each cell line from **H** are shown, colored by *CREBBP* mutation status. The ED_{50} for *CREBBP*-mutant (red) cell lines was significantly lower than that observed for *CREBBP* WT cell lines (blue; *t* test, $P = 0.002$). **J,** Gene-set enrichment analysis of "Germinal Center Terminal Differentiation" signature genes shows that these genes are coordinately induced in both *CREBBP* WT (above) and mutant (below) DLBCL cell lines by BRD3308 treatment compared with control.

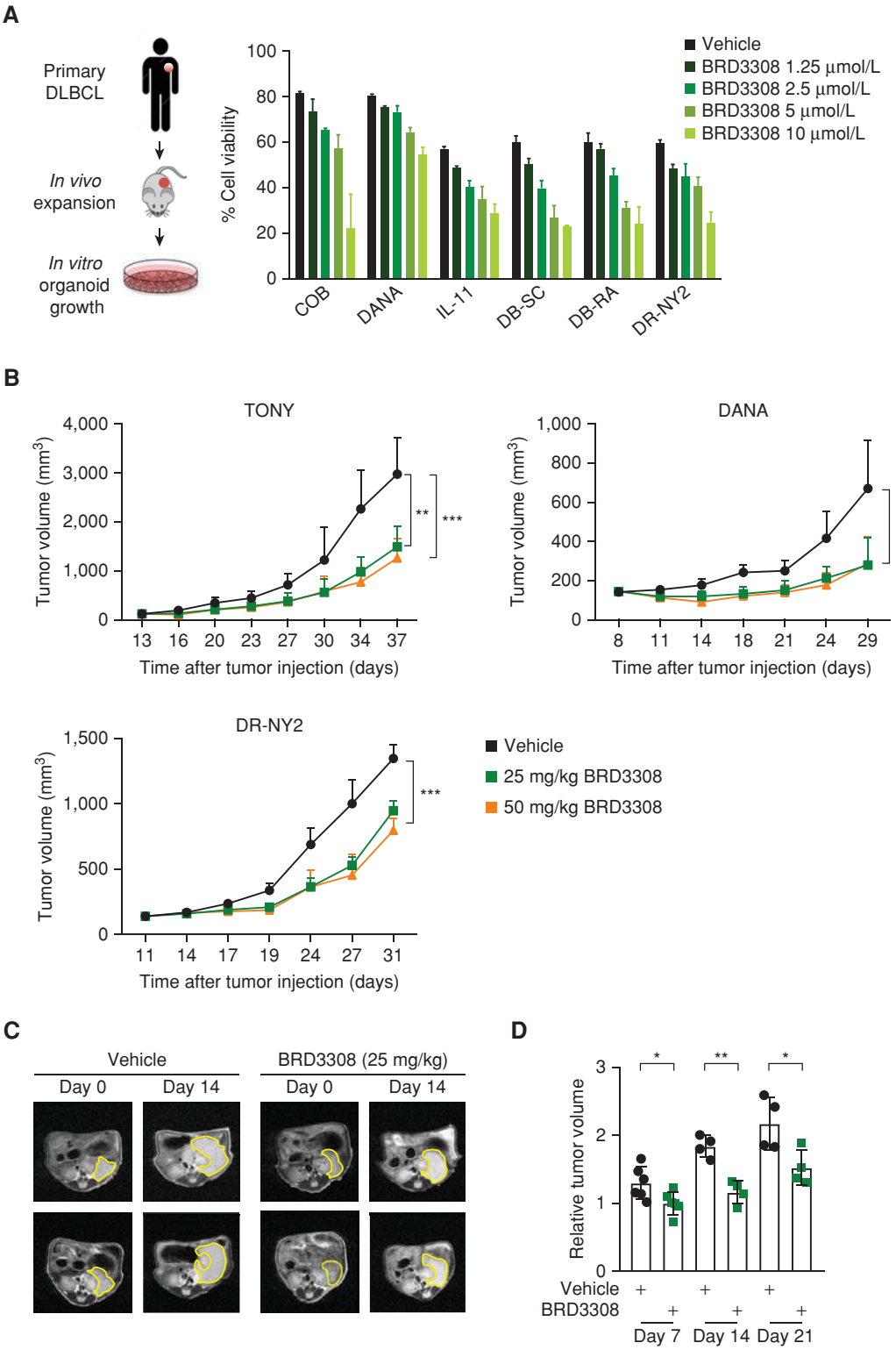

Figure 3. BRD3308 is effective in primary DLBCL. **A,** The sensitivity of primary DLBCL tumors to BRD3308 was evaluated by expanding them *in vivo*, followed by culture in our *in vitro* organoid model with different concentrations of BRD3308. A dose-dependent decrease in cell viability was observed in all 6 tumors with increasing concentrations of BRD3308. **B,** Treatment of three unique DLBCL xenograft models *in vivo* with 25 mg/kg (green) or 50 mg/kg (orange) of BRD3308 significantly reduced tumor growth compared with vehicle (black; **, $P < 0.01$; ***, $P < 0.001$). **C,** Representative MRI images of renal capsule implanted PDX tumors from a *CREBBP*^{R1446C}-mutant DLBCL at the beginning (day 0) and day 14 of treatment. Tumor is outlined in yellow. **D,** Quantification of tumor volume by MRI images, normalized to the pretreatment volume for the same tumor, shows that BRD3308 treatment significantly reduces tumor growth (*, $P < 0.05$; **, $P < 0.01$).

Downloaded from http://aacrjournals.org/cancerdiscovery/article-pdf/10/3/440/1813368/440.pdf by guest on 27 August 2022

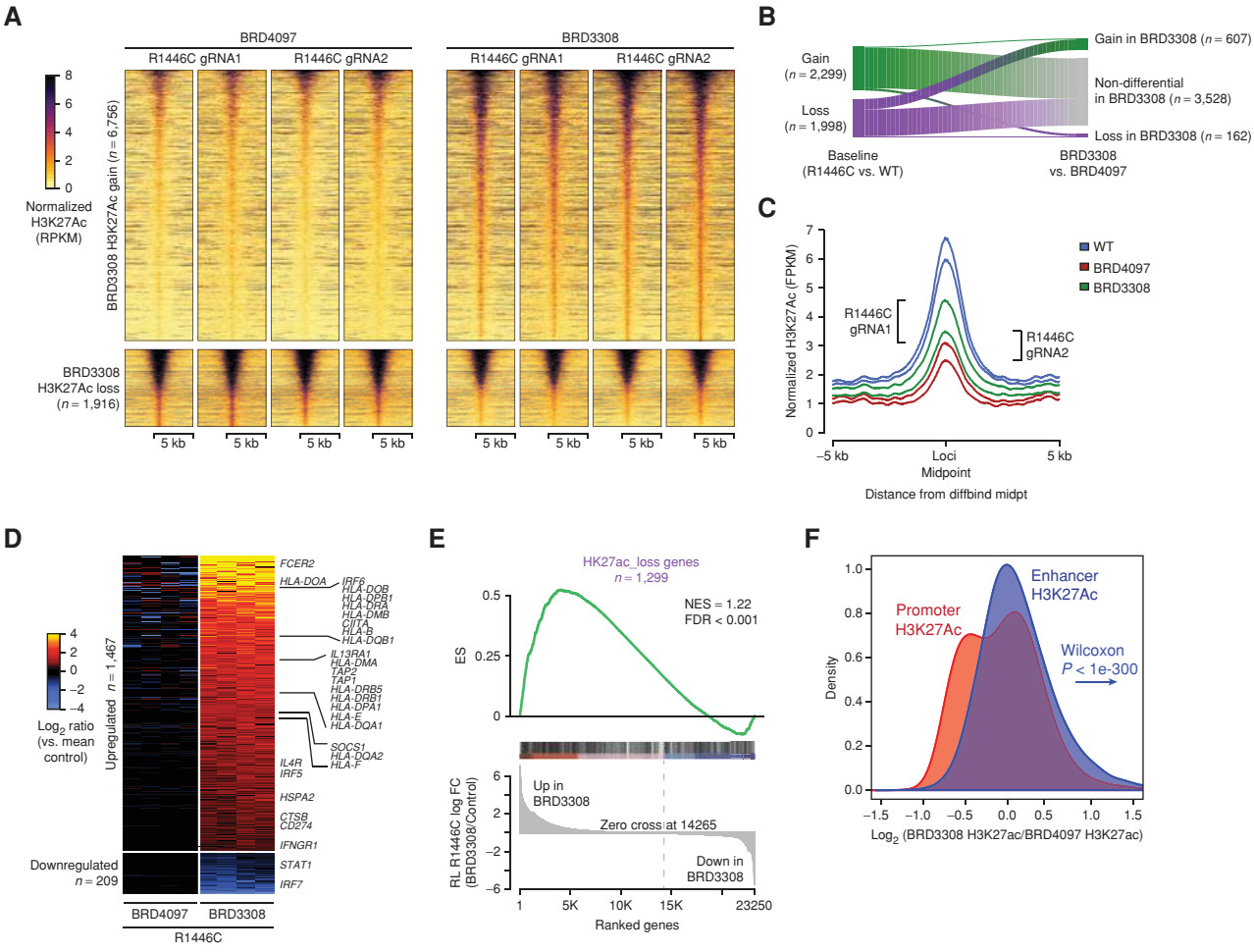

Figure 4. HDAC3 inhibition counteracts the molecular phenotype of *CREBBP* mutation. **A,** A heat map shows the regions with significantly increased (above, $n = 6,756$) or decreased (below, $n = 1,916$) H3K27Ac in *CREBBP*^{R1446C} cells treated with BRD3308 compared with those treated with the control compound, BRD4097. Experimental duplicates are shown for each clone. **B,** A river plot shows that a large fraction of the regions with significantly reduced H3K27Ac in *CREBBP*^{R1446C} cells compared with *CREBBP*^{WT} cells had significantly increased H3K27Ac following BRD3308 treatment. **C,** A density plot shows the regions with reduced H3K27Ac in *CREBBP*^{R1446C} compared with *CREBBP*^{WT} cells. The level of H3K27Ac over these regions is increased in *CREBBP*^{R1446C} cells treated with BRD3308 compared with control (BRD4097), but does not reach the level observed in *CREBBP*^{WT} cells. **D,** A heat map shows the genes with increased (above, $n = 1,467$) or decreased (below, $n = 209$) expression following BRD3308 treatment. Duplicate experiments are shown for each of the two *CREBBP*^{R1446C} clones. IFN-responsive genes, including those with a role in antigen processing and presentation, can be observed to increase in expression following BRD3308 treatment. **E,** Gene set enrichment analysis shows that the set of genes with reduced H3K27Ac in association with *CREBBP* mutation has coordinately increased expression following BRD3308 treatment. **F,** A density plot illustrates the relative change in promoter (red) and enhancer (blue) H3K27Ac following treatment with BRD3308, with the enhancer distribution being significantly more right-shifted (increased) compared with promoter regions. (*continued on next page*)

complexes, but were enriched in genes suppressed by *CREBBP* mutation and restored by HDAC3 inhibition. Given their critical role in antitumor immunity, we evaluated whether HDAC3 inhibition may be sufficient to restore or promote the expression of these BCL6-repressed immune signatures. Using MHC class II protein expression on *CREBBP*^{R1446C}-mutant cells as a proxy for the CREBBP/BCL6 counter-regulated IFN signaling pathway, we evaluated the activity of HDAC inhibitors for promoting the expression of immune response genes. Although HDAC inhibitors with broader specificities were able to induce MHC class II expression, selective inhibition of HDAC3 was sufficient for the robust and maximal (>10-fold) restoration of MHC class II expression in *CREBBP*^{R1446C} cells (Fig. 5A; Supplementary Fig. S12) in line with our observation that these genes are silenced by BCL6–HDAC3 complexes. These selective inhibitors each show some inhibition of other HDACs (28), and their activity in opposing BCL6 function may in part be linked to inhibition of HDAC1/2, which are recruited by BCL6 via CoRest and NuRD (4, 31, 32). However, HDAC1/2 have important functions in normal hematopoiesis (33), and hence compounds that target these enzymes induce toxic effects against these cells that are not elicited by BRD330829 (29), suggesting that selective inhibition of HDAC3 may limit hematologic toxicities that are observed with pan-HDAC inhibitors. Furthermore, although some of the less specific HDAC inhibitors were toxic to normal human CD4$^+$ and CD8$^+$ T cells, the selective inhibition of HDAC3 was not (Fig. 5B; Supplementary

Downloaded from http://aacrjournals.org/cancerdiscovery/article-pdf/10/3/440/1813368/440.pdf by guest on 27 August 2022

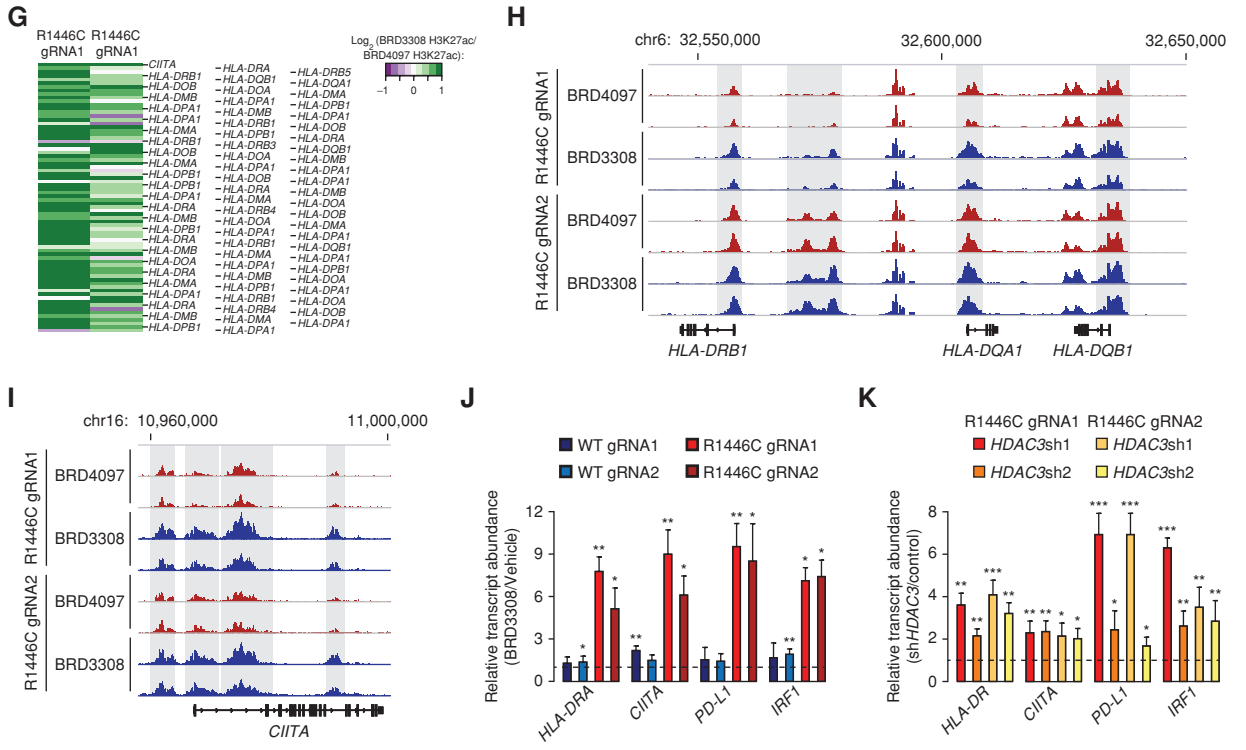

Figure 4. ***(Continued)*** **G,** A heat map shows the change in H3K27Ac at the promoter regions of MHC class II genes following BRD3308 treatment of *CREBBP*^{R1446C} cells, showing a coordinate increase. **H** and **I,** Regions with significantly increased H3K27Ac (shaded in gray) included those within the MHC class II and *CIITA* gene loci. **J,** The increased expression of candidate genes within the IFN signaling and antigen-presenting pathways was confirmed by qPCR. Increased expression was observed in both *CREBBP*^{WT} and *CREBBP*^{R1446C} cells following BRD3308 treatment, but the level of induction was much higher in *CREBBP*^{R1446C} cells. Data are shown relative to vehicle-treated cells (*t* test, *, $P < 0.05$; **, $P < 0.01$; ***, $P < 0.001$). **K,** The on-target role of HDAC3 in the induction of candidate genes was confirmed by shRNA-mediated knockdown of *HDAC3* and qPCR analysis of gene expression. Knockdown of *HDAC3* was able to induce the expression of all genes, which is shown relative the control shRNA (*t* test, *, $P < 0.05$; **, $P < 0.01$; ***, $P < 0.001$).

Fig. S13). This suggests that selective HDAC3 inhibition may be capable of eliciting immune responses by on-target on-tumor induction of antigen presentation without on-target off-tumor killing of T cells.

Based upon our observations with MHC class II, the magnitude of this induction appeared to be dependent upon the baseline of expression. We therefore hypothesized that *CREBBP* mutation status may determine the baseline expression for IFN and antigen-presenting pathways, but may not be a prerequisite for this response due to the conserved activity of BCL6–HDAC3 in regulating this axis in WT cells. We comprehensively evaluated this theory using our RNA-seq data from *CREBBP*^{WT} and *CREBBP*^{R1446C} cells treated with either the HDAC3 inhibitor BRD3308 or the inactive control compound BRD4097. Consistent with our observations of MHC class II protein expression, BRD3308 treatment coordinately induced the transcript expression of MHC class II and IFN pathway genes in both *CREBBP*^{WT} and *CREBBP*^{R1446C} CRISPR-edited cells (Fig. 5C). This trend included a significant enrichment for the genes that were epigenetically suppressed in association with *CREBBP* mutations, resulting in their significant increase in expression in *CREBBP*^{WT} cells (Fig. 5D), similar to our observations from *CREBBP*^{R1446C} cells (Fig. 4E). Moreover, we observed similar enrichment of transcriptionally induced pathways in both *CREBBP*^{WT} and *CREBBP*^{R1446C} cells that included the same pathways that were suppressed by *CREBBP* mutation (Fig. 5E; Supplementary Tables S7–S10). Consistent with the almost exclusive function of HDAC3 as a BCL6 corepressor in GC B cells (3), and the importance of BCL6 activity in both *CREBBP* WT and *CREBBP*-mutant cells, we observed highly significant enrichment for genes regulated by BCL6–SMRT complexes among genes with induced H3K27Ac and expression after BRD3308 treatment (Fig. 5E). Also significantly enriched were canonical BCL6 target gene sets such as p53-regulated genes, and signaling through BCR, CD40, and cytokines such as IL4 and IL10. Finally, we observed significant enrichment for BCL6 target gene sets linked to IFN signaling, antigen presentation via MHC class II, and PD-1 signaling.

Although there were conserved patterns of gene activation in both *CREBBP*^{WT} and *CREBBP*^{R1446C} cells, we observed that the magnitude of this induction was greatest in *CREBBP*^{R1446C} cells, which started from a lower baseline of expression linked to mutation-associated epigenetic suppression (Fig. 5F). We identified IRF1 as a BCL6-regulated transcription factor that is critical for IFN responses, and is induced by HDAC3 inhibition in *CREBBP*^{WT} and *CREBBP*^{R1446C} cells (Fig. 5C). We therefore hypothesized that IRF1 may contribute to the different magnitude of induction in MHC class II genes following HDAC3 inhibition in these two genetic contexts.

Downloaded from http://aacrjournals.org/cancerdiscovery/article-pdf/10/3/440/1813368/440.pdf by guest on 27 August 2022

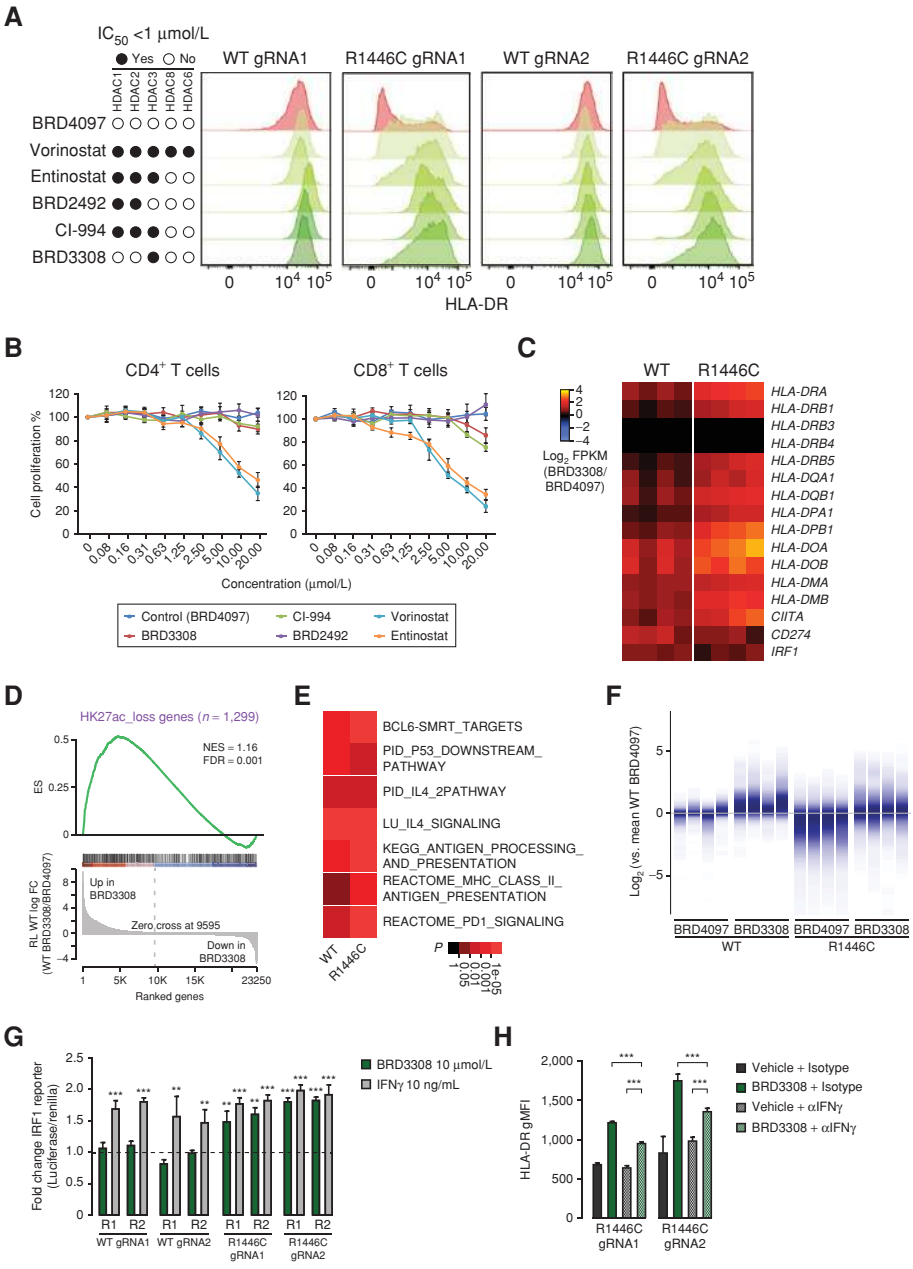

Figure 5. HDAC3 inhibition induces IFN signaling and antigen presentation in both *CREBBP* WT and *CREBBP*-mutant cells. **A,** Flow cytometry was performed for HLA-DR following exposure to a selection of HDAC inhibitors at 10 μmol/L for 72 hours. This shows that HDAC inhibitors with range specificities are able to induce MHC class II, but HDAC3-selective inhibition using BRD3308 is sufficient for this effect. **B,** Dose titrations of histone deacetylase inhibitors from **A** with peripheral blood CD4+ and CD8+ T cells from healthy donors. **C,** A heat map of IFN responsive and antigen-presenting genes from RNA-seq data shows an increased expression in both *CREBBP*^{WT} and *CREBBP*^{R1446C} cells. Data represent duplicate experiments for each clone and are normalized to control-treated cells from the same experiment. **D,** Gene set enrichment analysis of the genes that have reduced H3K27Ac in *CREBBP*^{R1446C} cells shows that the expression of these same genes is coordinately increased by BRD3308 treatment in *CREBBP*^{WT} cells. **E,** A heat map of hypergeometric enrichment analysis results of RNA-seq data shows that BRD3308 induces the induction of similar gene sets in both *CREBBP*^{WT} and *CREBBP*^{R1446C} cells. **F,** A density strip plot, normalized to the mean expression in control (BRD4097)-treated *CREBBP*^{WT} cells, shows the relative expression of the set of genes with reduced H3K27Ac in *CREBBP*^{R1446C} cells. This shows that these genes are induced by BRD3308 in *CREBBP*^{WT} cells, resulting in expression levels greater than baseline. Furthermore, *CREBBP*^{R1446C} cells can be observed to start below baseline, with the induction by BRD3308 resulting in expression levels similar to that observed in control-treated *CREBBP*^{WT} cells. The four samples per condition represent duplicate experiments in each of the two clones for each genotype. **G,** The firefly luciferase luminescence of two unique IRF1 reporters (R1 and R2) is shown, normalized to *Renilla* luciferase from a control vector and shown as fold change compared with untreated cells. *CREBBP*^{WT} cells show increased IRF1 activity following IFNγ treatment (positive control; gray), but not following treatment with BRD3308 (green). In contrast, *CREBBP*^{R1446C} cells show increased IRF1 activity following BRD3308 treatment, to a level that is similar to that observed with IFNγ treatment (*t* test vs. control-treated cells, **, $P < 0.01$; ***, $P < 0.001$). **H,** The role of IFNγ in inducing MHC class II expression following BRD3308 in *CREBBP*^{R1446C} cells was assessed with a blocking experiment. Blocking IFNγ with a neutralizing antibody (αIFNγ) significantly reduced the induction of MHC class II, as measured by flow cytometry for HLA-DR, but the induction by BRD3308 with αIFNγ remained significantly higher than vehicle with αIFNγ (*t* test, ***, $P < 0.001$).

Downloaded from http://aacrjournals.org/cancerdiscovery/article-pdf/10/3/440/1813368/440.pdf by guest on 27 August 2022

We investigated this by measuring IRF1 activity in a luciferase reporter assay in *CREBBP*^{WT} and *CREBBP*^{R1446C}-mutant cells. Treatment of *CREBBP*^{R1446C} cells with BRD3308 led to a significant increase of IRF1 activity that was similar in magnitude to that induced by IFNγ treatment (Fig. 5G). In contrast, this effect was not observed in isogenic *CREBBP*^{WT} control cells following HDAC3 inhibition, despite these cells showing similarly increased IRF1 activity in response to IFNγ treatment. Exposing *CREBBP*^{R1446C} cells to IFNγ-neutralizing antibodies only partially ameliorated MHC class II induction after BRD3308 in *CREBBP*-mutant cells (Fig. 5H). This suggests that preferential induction of antigen presentation by HDAC3 inhibition in *CREBBP*-mutant cells likely depends on a combination of mechanisms, including directly opposing BCL6 repression of these genes as well as secondary induction through IFNγ signaling (which is also directly regulated by BCL6).

HDAC3 Inhibition Restores MHC Class II Expression in Human DLBCL Cell Lines and Patient Specimens

The frequency of MHC class II loss in DLBCL exceeds the frequency of *CREBBP* mutations in this disease (13, 21), through unknown mechanisms. The ability of HDAC3 inhibition to induce MHC class II expression in *CREBBP* WT DLBCL cells may therefore have potentially broad implications for immunotherapy. Using RNA-seq data from WT (OCI-Ly1) and mutant (OCI-Ly19 and OZ) DLBCL cell lines (Fig. 6A; Supplementary Tables S11 and S12) and qPCR analysis of PDX tumors treated *in vivo* (Supplementary Fig. S14A–S14D), we confirmed that gene expression induced by HDAC3 inhibition was largely conserved in both contexts. The expression of *CD274* (encoding PD-L1) was significantly higher in 4 of 4 PDX tumors treated with 25 mg/kg BRD3308 *in vivo* compared with vehicle control–treated tumors, and MHC class II expression was significantly higher in 3 of 4 PDX tumors (Supplementary Fig. S14A–S14D). We extended upon this using IHC staining for MHC class II in tumors from a *CREBBP* R1446C–mutant PDX model (DFBL; Fig. 6B) and a *CREBBP* WT PDX model that was MHC class II negative at baseline (DR-NY2, Fig. 6C). In tumors from both models, *in vivo* treatment with BRD3308 led to a marked induction of MHC class II expression. In a broader panel of *CREBBP* WT and *CREBBP*-mutant cell lines, we observed that a core set of genes including *HLA-DR, CIITA*, and *CD274* had consistently higher expression in BRD3308-treated cells compared with the matched control, but with a higher magnitude of induction in *CREBBP*-mutant cell lines (Fig. 6D). This trend was also observed by flow cytometry for MHC class II, which extends upon our observations in CRISPR/Cas9-modified cells by showing a reproducible increase in expression in a larger panel of DLBCL cell lines, and a higher magnitude of induction in *CREBBP*-mutant cell lines (Fig. 6E). Together, these results show that selective inhibition of HDAC3 using BRD3308 can promote the expression of IFN and antigen-presenting pathway genes in both the *CREBBP* WT and *CREBBP*-mutant settings. However, the magnitude of induction is greatest in *CREBBP*-mutant cells, owing in part to the preferential induction of IRF1 activity in these cells.

HDAC3 Inhibition Drives T-cell Activation and Immune Responses

IFN signaling and antigen presentation are central to antitumor immune responses. We therefore investigated whether HDAC3 inhibition could promote antigen-dependent antitumor immunity. To test this, we implanted OCI-Ly18 DLBCL cells into NSG mice, and once tumors formed we injected human peripheral blood mononuclear cells (PBMC), including T cells, to expose them to antigens presented by the tumor cells. These are likely to be histocompatibility antigens rather than tumor neoantigens, but are nonetheless presented and recognized through MHC–T-cell receptor (TCR) interactions. After *in vivo* priming, tumor-infiltrating lymphocytes (TIL) were cocultured *in vitro* with OCI-Ly18 cells that were pretreated for 72 hours with increasing concentrations of BRD3308 to assess the effects on T-cell activation and tumor-cell killing (Fig. 7A). The DLBCL cells that were epigenetically primed for antigen presentation by BRD3308 significantly increased the activation of $CD4^+$ T cells, as determined by CD69 expression ($P < 0.05$; Fig. 7B). As in prior experiments, we observed cell-intrinsic effects of BRD3308 on OCI-Ly18 cells in the absence of TILs, resulting in declining cell viability with higher concentrations of the inhibitor. However, the effects of BRD3308 were markedly and significantly increased in the presence of TILs, consistent with T cell–directed killing of the tumor cells ($P < 0.001$; Fig. 7C). To confirm that this killing was dependent on MHC–TCR interactions, we also performed this experiment in the presence of blocking antibodies for MHC class I, MHC class II, or both. Blocking one or the other of MHC class I or II rescued some of the cytotoxicity observed in this assay, but blocking both MHC class I and class II together completely abrogated the TIL-associated effect (Fig. 7C). These data show that HDAC3 inhibition can potentiate antitumor immune responses that are likely to be antigen-dependent because they are driven by MHC–TCR interactions. Our identification of the IFN signaling pathway, and IFNγ itself, as a central component of the response to HDAC3 inhibition led us to test whether IFNγ levels may rise as a result of treatment. An ELISpot analysis of the IFNγ levels from the TIL and OCI-Ly18 coculture experiment revealed a striking and significant increase in IFNγ levels, even at the lowest concentrations of HDAC3 inhibitor (Fig. 7D; Supplementary Fig. S15).

Considering the manner in which to best harness the antilymphoma immunity effect of HDAC3 inhibitors, we noted that induction of MHC class II is mechanistically linked to IFNγ-associated PD-L1 upregulation, which could potentially limit maximal antitumor response. We therefore posited that PD-1/PD-L1 blockade may be an attractive combination regimen. To test this hypothesis, we used a murine lymphoma transplantation model in which splenocytes from *IμBcl6;Ezh2*^{Y641F} mice (5) were transplanted into irradiated syngeneic WT recipients (Fig. 7E). Aggressive tumors formed within these mice, which we treated with either vehicle control, BRD3308 alone, αPD-L1 alone, or a BRD3308 + αPD-L1 combination. Treatment with BRD3308 led to a significant increase in serum IFNγ within these mice, which was also observed with αPD-L1 treatment and was even further enhanced in an additive manner by the combination

Downloaded from http://aacrjournals.org/cancerdiscovery/article-pdf/10/3/440/1813368/440.pdf by guest on 27 August 2022

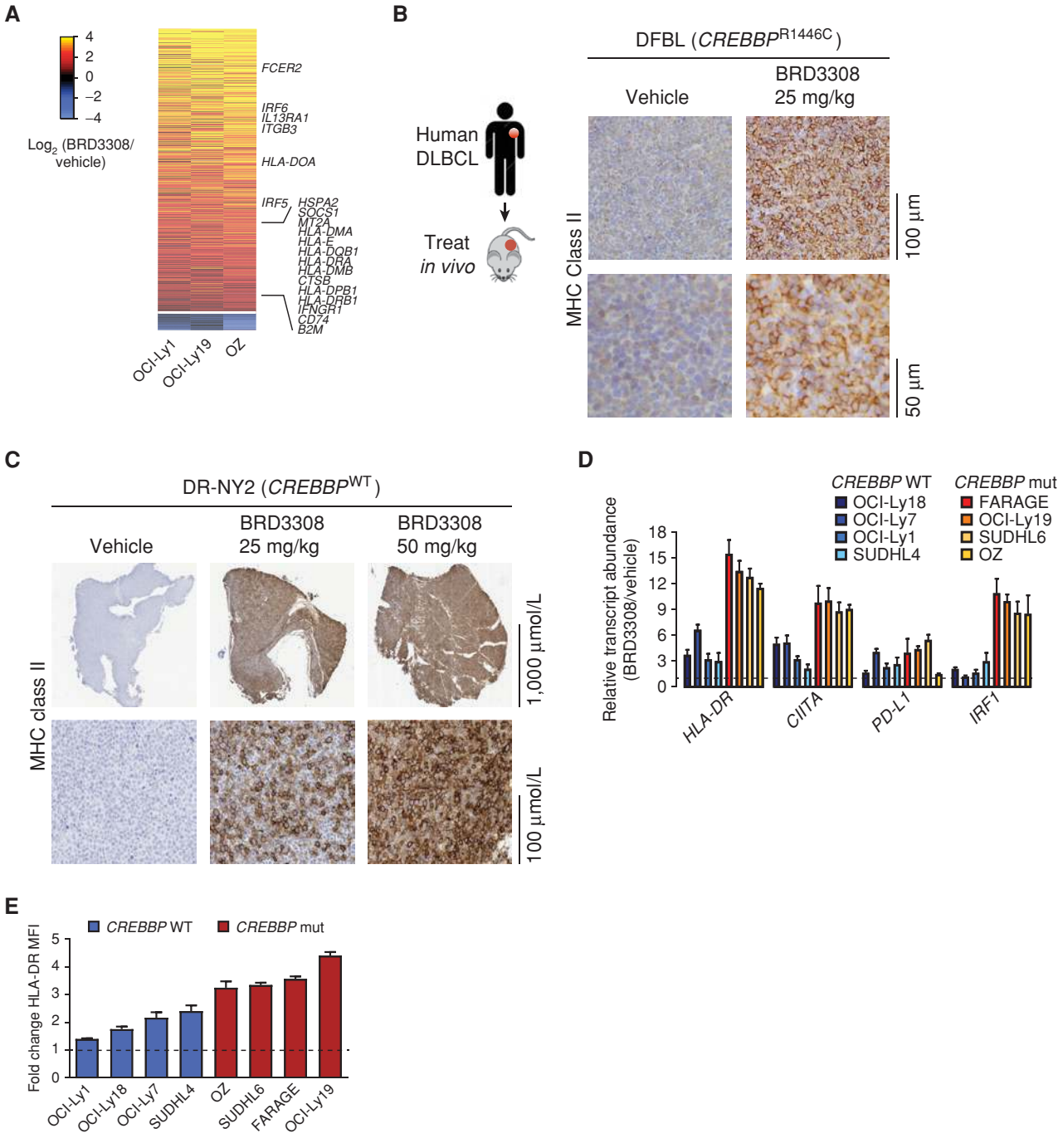

Figure 6. Induction of IFN-responsive and antigen-presenting genes in DLBCL cell lines and patient-derived xenografts. **A,** A heat map shows significantly upregulated (above) and downregulated (below) genes in BRD3308-treated DLBCL cell lines that are *CREBBP* WT (OCI-Ly1) or *CREBBP*-mutant (OCI-Ly19 and OZ), expressed as a $\log_2$ ratio to vehicle control–treated cells. The observed changes were consistent between WT and mutant cell lines, and included upregulation of IFN-responsive and antigen-presenting genes. **B,** MHC class II was assessed on vehicle control (left) and BRD3308-treated (25 mg/kg; right) tumors from a *CREBBP* R1446C–mutant PDX model, showing a visible increase in expression in the BRD3308-treated tumors. These images are representative of 4 tumors per group. **C,** An MHC class II–negative DLBCL patient-derived xenograft model was treated *in vivo* with either 25 mg/kg or 50 mg/kg of BRD3308. IHC staining was performed for MHC class II, revealing a robust induction of MHC class II expression that was relative to the dose of treatment. These images are representative of 6 tumors per group. **D,** qPCR was used to validate the gene expression changes of select IFN-responsive genes following BRD3308 treatment across an extended panel of *CREBBP* WT and *CREBBP*-mutant DLBCL cell lines. These genes were uniformly increased in both genetic contexts, but with a higher magnitude of increase in *CREBBP*-mutant cell lines. One-tailed Student *t* test, *, $P < 0.05$; **, $P < 0.01$; **, $P < 0.001$. **E,** The induction of MHC class II expression by BRD3308 was measured in an extended panel of DLBCL cell lines by flow cytometry. Data are plotted as a fold change of the mean fluorescence intensity (MFI) of HLA-DR in BRD3308-treated versus control-treated cells. We observed uniformly increased MHC class II expression in all cell lines, but with higher magnitude in *CREBBP* mutants.

Downloaded from http://aacrjournals.org/cancerdiscovery/article-pdf/10/3/440/1813368/440.pdf by guest on 27 August 2022

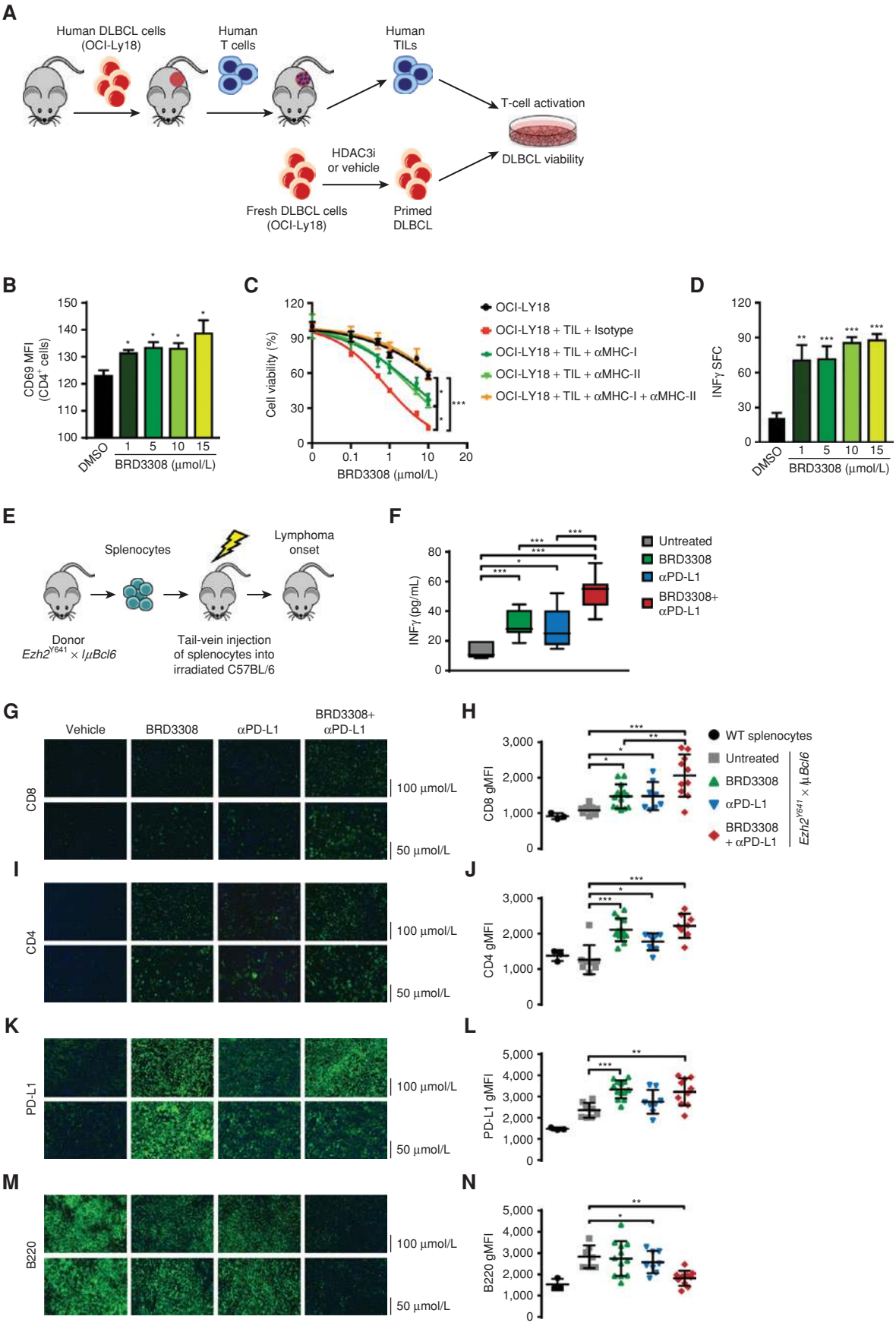

Downloaded from http://aacrjournals.org/cancerdiscovery/article-pdf/10/3/440/1813368/440.pdf by guest on 27 August 2022

treatment (Fig. 7F). Immunofluorescence staining for CD4 and CD8 showed significantly increased infiltration within the spleens from BRD3308-treated mice, which was further increased by the combination therapy (Fig. 7G–J). The ability of BRD3308 and αPD-L1 combination to increase TILs was likely linked with the IFNγ-mediated PD-L1 induction that was observed in BRD3308-treated tumors (Fig. 7K and L). In line with this interaction, BRD3308 and αPD-L1 each showed a small degree of single-agent efficacy, but the combination led to the most significant reduction in B220 cells within the spleens of tumor-bearing mice (Fig. 7M and N). Together, these data show that HDAC3 inhibitor–mediated reversal of the BCL6-repressed IFN pathway leads to joint induction of MHC class II and PD-L1, which, although eliciting significant antitumor immune response, can be further enhanced by combination with PD-1/PD-L1 blockade to yield a more potent immunotherapy strategy that is superior to immune checkpoint inhibition alone.

DISCUSSION

Precision medicine and immunotherapy have led to significant breakthroughs in a variety of cancers, but have lacked success in B-cell lymphoma. For precision medicine, this is largely due to a paucity of "actionable" genetic alterations or, rather, the lack of current therapeutic avenues to target the mutations that have been defined as being important for disease biology. For immunotherapy, the mechanisms driving lack of response or early progression are not well understood, but are likely to be underpinned by the complex immune microenvironment and genetic alterations that drive immune escape. The exception to both of these statements is the use of PD-1–neutralizing antibodies in classic Hodgkin lymphoma, which opposes genetically driven immune suppression by the malignant Reed–Sternberg cells through DNA copy-number gain of the PD-L1 locus (34) and elicits responses in the majority of patients (35). This stands as an example of the potential success that could be achieved by the characterization and rational therapeutic targeting of genetic alterations and/or the neutralization of immune escape mechanisms. However, we are not yet able to successfully target some of the most frequently mutated genes or overcome the barriers of inadequate response to immunotherapy in the most common subtypes of B-cell lymphoma. These are important areas of need if we hope to further improve the outcomes of these patients.

The *CREBBP* gene is mutated in approximately 15% of DLBCL (21) and approximately 66% of follicular lymphoma (7), and is therefore a potentially high-yield target for precision therapeutic approaches. Our use of CRISPR/Cas9 gene editing to generate isogenic lymphoma cell lines that differ only in their *CREBBP* mutation status allowed us to perform detailed characterization of the epigenetic and transcriptional consequences of these mutations. Using this approach, we identified for the first time functional differences between the most frequent KAT domain point mutation, R1446C mutations, and frameshift mutations that result in KO. Although similar regions of the genome showed reduced H3K27Ac in R1446C and KO mutants compared with isogenic WT controls, the magnitude of these changes was markedly reduced in *CREBBP* KO. This suggests that acetyltransferases such as EP300 may compensate for the loss of CREBBP protein in the setting of *CREBBP* nonsense/frameshift mutations, consistent with observations of functional redundancy between *Crebbp* and *Ep300* in B cell–specific conditional KO mice (25, 36). But the presence of a catalytically inactive $CREBBP^{R1446C}$ protein may dominantly suppress histone acetylation by preventing the participation of redundant acetyltransferases such as EP300 in transcriptional activating complexes. This yields a more severe epigenetic and transcriptional phenotype in $CREBBP^{R1446C}$ mutants compared with $CREBBP^{KO}$ mutants, and an inferior clinical outcome.

Despite differences in the magnitude of molecular changes between R1446C and KO cells, these mutations yielded a similar degree of synthetic vulnerability to HDAC3 inhibition. This was likely driven by the increased suppression of BCL6 target genes that we observed in both contexts, including *CDKN1A* (encoding p21). This gene has also been highlighted as a critical nexus in the oncogenic potential of *EZH2* (37), which cooperates with BCL6 to silence gene expression (5). One of the important mechanisms for BCL6-mediated gene silencing is through the recruitment of HDAC3 as part of the NCOR/SMRT complex (3), thereby highlighting HDAC3 inhibition as a rational therapeutic avenue for counteracting BCL6 activity. Virtually all of the HDAC3 corepressor complexes present in DLBCL cells are bound with BCL6, suggesting that HDAC3 inhibitors' effect is largely explained by their depression of the subset of BCL6 target genes

Figure 7. HDAC3 inhibition induces antigen-dependent immune responses. **A,** A schematic of the generation of antigen-specific T cells and epigenetic priming of DLBCL cells. A human DLBCL cell line (OCI-Ly18) was engrafted into immunodeficient mice and allowed to establish. Human T cells were then engrafted, exposing them to tumor antigens prior to harvesting of the tumor-infiltrating T-cell (TIL) fraction. These TILs were cultured with fresh DLBCL cells that had been epigenetically primed with different concentrations of BRD3308, and the cell viability of the DLBCL cells was measured after 72 hours. **B,** TIL and DLBCL coculture resulted in activation of the $CD4^+$ T cells in a dose-dependent manner, as measured by flow cytometry for the CD69 activation marker. Data represent the fold change in CD69 expression compared with vehicle-treated DLBCL cells (*t* test vs. DMSO control, *, $P < 0.05$). **C,** The cell viability of DLBCL cells in TIL coculture experiments was measured by CellTiter-Blue assay. Treatment with BRD3308 resulted in some cell killing through cell-intrinsic mechanisms in the absence of TILs (black). The addition of TILs at a 1:1 ratio led to a significant increase in cell death of the DLBCL cells. This was partially reduced by blocking of either MHC class I or MHC class II using neutralizing antibodies. Blocking of MHC class I and class II together completely eliminated the TIL-associated increase in cell death, suggesting that killing was mediated through MHC–TCR interactions (*t* test, *, $P < 0.05$; ***, $P < 0.001$). **D,** The production of IFNγ was measured by ELISpot and found to increase in cultures with epigenetically primed DLBCL cells (*t* test vs. DMSO control, **, $P < 0.01$; ***, $P < 0.001$). SFC, spot-forming cells. **E,** A syngeneic BCL6-dependent lymphoma model for *in vivo* testing of BRD3308 and PD-L1–blocking antibodies. Splenocytes were taken from $Ezh2^{Y641}$;*IμBcl6* mice and injected into irradiated WT recipients that were treated upon the onset of lymphoma. **F,** Serum IFNγ levels measured in mice following treatment. **G–N,** Representative immunofluorescence images of mouse spleens following treatment and quantification of mean fluorescence intensities (MFI) from multiple mice for CD8 (**G** and **H**), CD4 (**I** and **J**), PD-L1 (**K** and **L**), and B220 (**M** and **N**), showing increased T-cell infiltration following treatment with BRD3308 and cooperation with αPD-L1 in eliminating $B220^+$ tumor cells within the spleen (*t* test, *, $P < 0.05$; **, $P < 0.01$; ***, $P < 0.001$).

Downloaded from http://aacrjournals.org/cancerdiscovery/article-pdf/10/3/440/1813368/440.pdf by guest on 27 August 2022

regulated through this mechanism (3). Importantly, as a variety of GCB-derived malignancies rely on BCL6 function independently of *CREBBP* or *EZH2* mutation (38, 39), opposing this function through HDAC3 inhibition may also be effective in tumors without these genetic alterations. We have shown preliminary evidence in the primary setting using DLBCL PDX models.

One of the important transcriptional programs that is regulated by BCL6 is the IFN signaling pathway (3), which we observed to be significantly repressed in *CREBBP*-mutant cells. It has been also long been recognized that IFNγ cooperates with lymphocytes to prevent cancer development (40). IFN signaling supports T cell–driven antitumor immunity via a variety of mechanisms, including the induction of antigen presentation on MHC class II (41), and the expression of MHC class II–restricted tumor antigens is required for the spontaneous or immunotherapy-induced rejection of tumors (14). We have shown that the selective inhibition of HDAC3 is sufficient for broadly restoring the reduced H3K27Ac and gene expression that is associated with *CREBBP* mutation, including the IFN signaling and antigen-presenting programs. This was in part driven by the increased production of IFNγ following HDAC3 inhibition, but also via the induced expression and activity of the IRF1 transcription factor. Together, these factors led to a robust restoration of MHC class II expression on *CREBBP*-mutant cells and drove dose-dependent potentiation of antitumor T-cell responses. However, we also noted that the same molecular signature is promoted by HDAC3 inhibition in *CREBBP* WT cells, also with an associated increase of MHC class II expression. As with the cell-intrinsic effects of HDAC3 inhibition, the effects on immune interactions may therefore be active in both *CREBBP* WT and *CREBBP*-mutant cells as a result of the conserved molecular circuitry controlling these pathways in each genetic context.

A variety of HDAC inhibitors were capable of restoring antigen presentation in our models, and clinical responses are observed with these agents in patients with relapsed/refractory follicular lymphoma and DLBCL. However, grade 3 to 4 hematologic toxicities such as thrombocytopenia, anemia, and neutropenia were frequent, and the responses tended not to be durable (42, 43). We posit that specific inhibition of HDAC3 may be accompanied by reduced toxicity, as HDAC1 and HDAC2 have important roles in hematopoiesis (33), and avoiding the inhibition of these HDACs may therefore avoid the undesired hematologic effects associated with pan-HDAC inhibition. In line with this, we observed that BRD3308 was less toxic to $CD4^+$ and $CD8^+$ T cells than pan-HDAC inhibitors, and was able to elicit MHC-dependent T-cell responses against a *CREBBP* WT DLBCL cell line *in vitro*. Although these responses are likely driven by histocompatibility antigens rather than tumor neoantigens, they support the premise that selective HDAC3 inhibition is capable of promoting antigen presentation and immune responses. We also speculate that the clinically observed lack of durability for HDAC inhibitors may be the result of adaptive immune suppression through mechanisms such as PD-L1 induction, which dampens T-cell responses through the PD-1 receptor (44), as well as direct toxicity of pan-HDAC inhibitors to T cells. We found evidence for adaptive immune suppression within our model systems, showing that HDAC3 inhibition leads to increased IFNγ production and the upregulation of *PD-L1* expression. This is in line with recent observations that *CD274* (encoding PD-L1) is a BCL6-supressed gene (45) and with a well-characterized role for PD-L1 as an IFNγ-responsive gene (44). In other cancers in which a florid antigen-driven immune response and concomitant adaptive immune suppression via PD-L1 exist within the tumor microenvironment, blockade of the PD-1 receptor is an effective therapeutic strategy (15, 17). Recent studies have also shown that the efficacy of PD-1 blockade is inextricably linked with the existence of an IFN-driven immune response and expression of MHC class II (15, 17). We have shown some evidence for this in a syngeneic, BCL6-driven murine model of B-cell lymphoma, wherein the combination of HDAC3 inhibition and αPD-L1 led to enhanced levels of $CD4^+$ and $CD8^+$ T-cell infiltration and clearance of tumor cells. Together, these observations suggest that the greatest potentiation of antitumor immunity in GCB-derived malignancies may be achieved through stimulation of IFN signaling and MHC class II expression by HDAC3 inhibition, in combination with the blockade of adaptive immune suppression using PD-L1/PD-1 neutralizing antibodies. However, this concept requires further exploration in future studies.

In conclusion, this work defines a molecular circuit that controls the survival and differentiation of lymphoma B cells and their interaction with T cells. This circuit is antagonistically regulated by CREBBP and BCL6, and can be pushed toward promoting tumor cell death and antitumor immunity via selective inhibition of HDAC3. This highlights HDAC3 inhibition as an attractive therapeutic avenue, which may be broadly active in follicular lymphoma and DLBCL due to the near-ubiquitous role of BCL6, but which may have enhanced potency in *CREBBP*-mutant tumors.

METHODS

For detailed methods, please refer to the Supplementary Methods.

CRISPR/Cas9 Modification of Lymphoma Cells

The RL cell line (ATCC CRL-2261) was modified by electroporation with one of two unique gRNA sequences in the pSpCas9(BB)-2A-GFP vector (Addgene plasmid #48138, gift from Feng Zhang, Massachusetts Institute of Technology; ref. 46) with a single-stranded oligonucleotide donor template. Single GFP-positive cells were sorted 3 to 4 days after transfection, and colonies expanded and evaluated for changes in the targeted region using Sanger sequencing. The process was repeated until point mutants were retrieved from cells treated with each of the two gRNAs, totaling 742 single clones. Potential off-target sites of each gRNA were determined by BLAST, and all sites with ≥16/20 nucleotide match to either of the gRNA sequences were interrogated by Sanger sequencing (Supplementary Table S13). All cells were maintained as subconfluent culture in RPMI medium with 10% FBS and penicillin/streptomycin and revalidated by Sanger sequencing prior to each set of experiments. Basic phenotyping of the cell lines is presented in Supplementary Fig. S16A–S16E.

ChIP-seq

Cells were washed and fixed in formaldehyde and chromatin sheared by sonication. An antibody specific to H3K27Ac (Active Motif) was coupled to magnetic protein G beads and incubated with chromatin overnight, and immunoprecipitation was performed.

Downloaded from http://aacrjournals.org/cancerdiscovery/article-pdf/10/3/440/1813368/440.pdf by guest on 27 August 2022

Input controls were reserved for comparison. Nucleosomal DNA was isolated and used either as a template for qPCR (ChIP-qPCR) or to generate NGS libraries using KAPA Hyper Prep Kits (Roche) and TruSeq adaptors (Bioo Scientific) using 6 cycles of PCR enrichment. Libraries were 6-plexed and sequenced with 2 × 100bp reads on a HiSeq-4000 (Illumina). The data were mapped using BWA, peaks called using MACS2, and differential analyses performed using DiffBind. For GSEA, the gene with the closest transcription start site to the peak was used. The statistical thresholds for significance were $q < 0.05$ and fold change > 1.5.

RNA-seq

Total RNA was isolated using AllPrep DNA/RNA Kits (Qiagen) and evaluated for quality on a Tapestation 4200 instrument (Agilent). Total RNA (1 μg) was used for library preparation with KAPA HyperPrep RNA Kits with RiboErase (Roche) and TruSeq adapters (Bioo Scientific). Libraries were validated on a Tapestation 4200 instrument (Agilent), quantified by Qubit dsDNA Kit (Life Technologies), 6-plexed, and sequenced on a HiSeq4000 instrument at the MD Anderson Sequencing and Microarray Facility using 2 × 100 bp reads. Reads were aligned with STAR, and differential gene expression analysis performed with DEseq2. The statistical thresholds for significance were $q < 0.05$ and fold change > 2.

Cell Proliferation Assays

Cells were seeded in 96-well plates at 50,000 cells/100 μL/well with either vehicle (DMSO 0.1%) or increasing concentrations of drugs. Cell viability was assessed with the fluorescent redox dye CellTiter-Blue (Promega). The reagent was added to the culture medium at 1:5 dilution, according to the manufacturer's instructions. Procedures to determine the effects of certain conditions on cell proliferation and apoptosis were performed in three independent experiments. The two-tailed Student *t* test and Wilcoxon rank-sum test were used to estimate the statistical significance of differences among results from the three experiments. Significance was set at $P < 0.05$. The PRISM software was used for the statistical analyses.

PDX and In Vitro *Organoid Studies*

A *CREBBP* R1446C–mutant tumor (DFBL13727) was obtained from the public repository of xenografts (47), expanded for 12 weeks in 1 mouse by surgical implantation into the renal capsule, and then implanted into the renal capsule of 12 additional mice for efficacy studies. Tumors were allowed to grow for 6 weeks, the size measured by MRI, and mice randomized to treatment and control groups to similar average tumor sizes. Mice were treated with BRD3308 (25 mg/kg) or vehicle control twice per day, 5 days on and 2 days off for a total of 3 weeks, and tumor size was assessed by MRI every 7 days. Two mice per group were euthanized on day 10 and the tumors harvested for biomarker analysis. Mice were cared for in accordance with guidelines approved by the MD Anderson Institutional Animal Care and Use Committee.

For *CREBBP* WT tumors (NY-DR2, DANA, and TONY), 6-week-old female NSG mice were implanted subcutaneously and treatments started when tumors reached 100 mm^3. Mice (12/group) were randomized and dosed via oral gavage with BRD3308 (25 mg/kg) or control vehicle (0.5% methylcellulose, 0.2% Tween 80) twice daily for 21 consecutive days. Mice were cared for in accordance with guidelines approved by the Memorial Sloan Kettering Cancer Center Institutional Animal Care and Use Committee and Research Animal Resource Center.

For *in vitro* organoid culture, the tumors were dissociated in single cells, stained with carboxyfluorescein diacetate succinimidyl ester (CFSE), washed, and mixed with irradiated 40LB cells at a 10:1 ratio of Primary:40LB. The cell mixture was then used to fabricate organoids in a 96-well plate as described previously (48), with 20 μL organoids containing 3% silicate nanoparticles and a 5% gelatin in Iscove's Modified Dulbecco's Medium (IMDM) solution. The organoids were cultured in IMDM containing 20% FBS supplemented with antibiotics and normocin (Invivogen) for 6 days, doubling the volume of medium after 3 days. The cell mixture was exposed to four 1:3 serial dilutions of BRD3308 starting at 5 μmol/L or vehicle control (DMSO) in triplicate for 6 days, treating a second time at 3 days. After 6 days of exposure, cell viability and proliferation were assessed by flow cytometry using DAPI staining gating on CFSE-positive cells.

Ex Vivo *Killing Assay*

The OCI-LY18 cells were subcutaneously implanted in NSG mice and allowed to become established before the mice were injected with PBMC. After 2 weeks, the tumors were dissociated to single cells and $CD3^+$ TILs were positively selected. T cells were expanded with a single administration of immunomagnetic microbeads coated with mouse anti-human CD3 and CD28 mAbs and rhIL2 and rhIL15 for 5 days. OCI-LY18 cells were treated with either DMSO or 10 μmol/L BRD3308 for 3 days, washed, and resuspended in fresh media with or without T cells at a ratio of 1:10. For MHC blocking, OCI-LY18 cells were treated with 10 μg/mL of either isotype Ig or blocking antibody against HLA-ABC W6/32, HLA-DR/DP/DQ, or the combination of the two. After 24-hour coculture, cell viability was analyzed using CellTiter-Blue.

Immunocompetent IμBcl6;Ezh2^{Y641F} *Model*

Six-week-old female C56BL/6J mice were irradiated at day −1 and 0 with 250 rad, and after 2 hours transplanted with 1×10^6 splenocytes from *IμBcl6;Ezh2*^{Y641F} mice (5) and 0.2×10^6 bone marrow cells from a healthy age-matched donor. Three weeks after transplantation, mice became sick and treatment was initiated with either vehicle or BRD3308 (25 mg/kg twice daily, every day for 21 days) via oral gavage, with or without αPD-L1 delivered by intraperitoneal injection (250 μg twice weekly for 4 administration). Mice were monitored daily and euthanized when they became moribund. Spleen and liver were measured, weighed, and analyzed by flow cytometry for evaluating the disease. Immunofluorescence staining and imaging were performed at the Molecular Cytology Core Facility of Memorial Sloan Kettering Cancer Center (New York, NY). Sections were stained with either anti-CD4 (R&D Systems, catalog no. AF554, 2 μg/mL) or anti–PD-L1 (R&D Systems catalog no. AF1019, 2 μg/mL) or B220 (BD Bioscience, catalog no. 550286, 0.3 μg/mL) or anti-CD8 (eBiosciences catalog no. 14–0808, 2.5 μg/mL) for 5 hours, followed by 60-minute incubation with biotinylated horse anti-goat IgG (for CD4 and PD-L1; Vector Laboratories, catalog no. BA-9500) or biotinylated goat anti-rat IgG (for CD8 and B220; Vector Laboratories, catalog no. BA9400) at 1:200 dilution. The detection was performed with Streptavidin-HRP D (part of DAB Map kit, Ventana Medical Systems), followed by incubation with Tyramide Alexa 488 (Invitrogen, catalog no. B40953), and counterstaining with DAPI (Sigma Aldrich, catalog no. D9542, 5 μg/mL). The slides were scanned with a Pannoramic Flash P250 Scanner (3DHistech) using a 20×/0.8NA objective lens. The fluorescence channels were imaged using DAPI, FITC, and TRITC filters sequentially with manually adjusted exposure times. Images were then exported into .tifs using Caseviewer (3DHistech) to be analyzed.

Data Deposition

The RNA-seq and ChIP-seq data are available at the Gene Expression Omnibus database under accession number GSE142357.

Disclosure of Potential Conflicts of Interest

A.Y. Chang is a postdoctoral fellow at Pfizer Inc. (but was not during the time of this manuscript study). S.S. Neelapu is a consultant at Kite/Gilead, Novartis, Incyte, Legend Biotech, Merck, Celgene,

Downloaded from http://aacrjournals.org/cancerdiscovery/article-pdf/10/3/440/1813368/440.pdf by guest on 27 August 2022

Unum Therapeutics, Pfizer, Precision Biosciences, Cell Medica, Allogene, and Calibr and reports receiving commercial research grants from Kite/Gilead, Novartis, Merck, BMS, Cellectis, Poseida, Karus, Acerta, Allogene, and Unum Therapeutics. J. Baselga is an EVP, Oncology R&D, at AstraZeneca, is a member of the Board of Directors at Foghorn, Varian Medical Systems, and Bristol-Myers Squibb, is a consultant for Grail, Aura, Infinity, PMV Pharma, Juno, and Seragon, reports receiving a commercial research grant from Roche, and has ownership interest (including patents) in Apogen, Tango, and Venthera. A. Younes is a consultant at Xynomics, BMS, Merck, and Janssen. A. Dogan is a consultant at Roche, Seattle Genetics, EUSA Pharma, Takeda, and Corvus Pharmaceuticals, reports receiving a commercial research grant from Roche, and is a consultant/advisory board member for Amgen. D.A. Scheinberg is on the SAB at Eureka, Oncopep, KLUS, Sellas, Actinium, and Pfizer, reports receiving a commercial research grant from BMS, and has ownership interest (including patents) in IOVA. A.M. Melnick is a consultant for Epizyme and Constellation, reports receiving commercial research grants from Janssen and Daiichi Sankyo, and is a consultant/advisory board member for KDAC. M.R. Green is a consultant at Verastem Oncology, has ownership interest (including patents) in KDAC Therapeutics, and is a consultant/advisory board member for KDAC Therapeutics. No potential conflicts of interest were disclosed by the other authors.

Authors' Contributions

Conception and design: P. Mondello, S. Tadros, E. de Stanchina, J. Baselga, A.M. Melnick, M.R. Green

Development of methodology: P. Mondello, S. Tadros, H.-Y. Ying, E. Toska, A.M. Melnick, M.R. Green

Acquisition of data (provided animals, acquired and managed patients, provided facilities, etc.): P. Mondello, S. Tadros, L. Fontan, A.Y. Chang, N. Jain, H. Yang, S. Singh, H.-Y. Ying, C.-S. Chu, S. Alig, M. Durant, E. de Stanchina, S. Ghosh, A. Mottok, S.S. Neelapu, O. Weigert, G. Inghirami, A. Younes, A. Dogan, R.G. Roeder, A.M. Melnick

Analysis and interpretation of data (e.g., statistical analysis, biostatistics, computational analysis): P. Mondello, S. Tadros, M. Teater, L. Fontan, A.Y. Chang, H. Yang, H.-Y. Ying, C.-S. Chu, M.C.J. Ma, S. Alig, S. Ghosh, A. Mottok, L. Nastoupil, S.S. Neelapu, O. Weigert, J. Baselga, A. Dogan, D.A. Scheinberg, R.G. Roeder, A.M. Melnick, M.R. Green

Writing, review, and/or revision of the manuscript: P. Mondello, S. Tadros, M. Teater, H.-Y. Ying, A. Mottok, L. Nastoupil, S.S. Neelapu, G. Inghirami, J. Baselga, A. Younes, C. Yee, D.A. Scheinberg, A.M. Melnick, M.R. Green

Administrative, technical, or material support (i.e., reporting or organizing data, constructing databases): P. Mondello, M.C.J. Ma, L. Nastoupil, S.S. Neelapu, A.M. Melnick, M.R. Green

Study supervision: A. Younes, D.A. Scheinberg, A.M. Melnick, M.R. Green

Acknowledgments

This work was supported by R01 CA201380 (to M.R. Green), R01 CA055349 (to D.A. Scheinberg), R01 CA178765 (to R.G. Roeder), U54 OD020355 01 (to E. de Stanchina and G. Inghirami), NCI SPORE P50 CA192937 (to A. Dogan and A. Younes), the MD Anderson Cancer Center (P30 CA016672) and Memorial Sloan Kettering Cancer Center (P30 CA008748) NCI CORE Grants, the Chemotherapy Foundation (to A.M. Melnick), the Star Cancer Consortium (to A.M. Melnick), the Jaime Erin Follicular Lymphoma Research Consortium (to A.M. Melnick, M.R. Green, and S.S. Neelapu), the Schweitzer Family Fund (to M.R. Green), and the Futcher Foundation (to L. Nastoupil and M.R. Green). H. Yang is a Fellow of the Leukemia and Lymphoma Society.

Received January 29, 2019; revised November 11, 2019; accepted January 3, 2020; published first January 8, 2020.

REFERENCES

1. Hatzi K, Melnick A. Breaking bad in the germinal center: how deregulation of BCL6 contributes to lymphomagenesis. Trends Mol Med 2014;20:343–52.
2. Mesin L, Ersching J, Victora GD. Germinal center B cell dynamics. Immunity 2016;45:471–82.
3. Hatzi K, Jiang Y, Huang C, Garrett-Bakelman F, Gearhart MD, Giannopoulou EG, et al. A hybrid mechanism of action for BCL6 in B cells defined by formation of functionally distinct complexes at enhancers and promoters. Cell Rep 2013;4:578–88.
4. Hatzi K, Geng H, Doane AS, Meydan C, LaRiviere R, Cardenas M, et al. Histone demethylase LSD1 is required for germinal center formation and BCL6-driven lymphomagenesis. Nat Immunol 2019;20:86–96.
5. Beguelin W, Teater M, Gearhart MD, Calvo Fernández MT, Goldstein RL, Cárdenas MG, et al. EZH2 and BCL6 cooperate to assemble CBX8-BCOR complex to repress bivalent promoters, mediate germinal center formation and lymphomagenesis. Cancer Cell 2016;30:197–213.
6. Green MR. Chromatin modifying gene mutations in follicular lymphoma. Blood 2018;131:595–604.
7. Green MR, Kihira S, Liu CL, Nair RV, Salari R, Gentles AJ, et al. Mutations in early follicular lymphoma progenitors are associated with suppressed antigen presentation. Proc Natl Acad Sci U S A 2015;112:E1116–25.
8. Jiang Y. Ortega-Molina A, Geng H, Ying HY, Hatzi K, Parsa S, et al. CREBBP inactivation promotes the development of HDAC3-dependent lymphomas. Cancer Discov 2017;7:38–53.
9. Allen CD, Okada T, Cyster JG. Germinal-center organization and cellular dynamics. Immunity 2007;27:190–202.
10. Khodadoust MS, Olsson N, Wagar LE, Haabeth OA, Chen B, Swaminathan K, et al. Antigen presentation profiling reveals recognition of lymphoma immunoglobulin neoantigens. Nature 2017;543:723–7.
11. Khodadoust MS, Olsson N, Chen B, Sworder B, Shree T, Liu CL, et al. B cell lymphomas present immunoglobulin neoantigens. Blood 2019;133:878–81.
12. Marty R, Thompson WK, Salem RM, Zanetti M, Carter H. Evolutionary pressure against MHC class II binding cancer mutations. Cell 2018;175:416–28.
13. Rimsza LM, Roberts RA, Miller TP, Unger JM, LeBlanc M, Braziel RM, et al. Loss of MHC class II gene and protein expression in diffuse large B-cell lymphoma is related to decreased tumor immunosurveillance and poor patient survival regardless of other prognostic factors: a follow-up study from the Leukemia and Lymphoma Molecular Profiling Project. Blood 2004;103:4251–8.
14. Alspach E, Lussier DM, Miceli AP, Kizhvatov I, DuPage M, Luoma AM, et al. MHC-II neoantigens shape tumour immunity and response to immunotherapy. Nature 2019;574:696–701.
15. Rodig SJ, Gusenleitner D, Jackson DG, Gjini E, Giobbie-Hurder A, Jin C, et al. MHC proteins confer differential sensitivity to CTLA-4 and PD-1 blockade in untreated metastatic melanoma. Sci Transl Med 2018;10:eaar3342.
16. Ayers M, Lunceford J, Nebozhyn M, Murphy E, Loboda A, Kaufman DR, et al. IFN-gamma-related mRNA profile predicts clinical response to PD-1 blockade. J Clin Invest 2017;127:2930–40.
17. Tumeh PC, Harview CL, Yearley JH, Shintaku IP, Taylor EJ, Robert L, et al. PD-1 blockade induces responses by inhibiting adaptive immune resistance. Nature 2014;515:568–71.
18. Borst J, Ahrends T, Babala N, Melief CJM, Kastenmuller W. CD4(+) T cell help in cancer immunology and immunotherapy. Nat Rev Immunol 2018;18:635–47.
19. Garcia-Ramirez I, Tadros S, González-Herrero I, Martín-Lorenzo A, Rodríguez-Hernández G, Moore D, et al. Crebbp loss cooperates with Bcl2 over-expression to promote lymphoma in mice. Blood 2017;129:2645–56.

Downloaded from http://aacrjournals.org/cancerdiscovery/article-pdf/10/3/440/1813368/440.pdf by guest on 27 August 2022

20. Mullighan CG, Zhang J, Kasper LH, Lerach S, Payne-Turner D, Phillips LA, et al. CREBBP mutations in relapsed acute lymphoblastic leukaemia. Nature 2011;471:235–9.
21. Pasqualucci L, Dominguez-Sola D, Chiarenza A, Fabbri G, Grunn A, Trifonov V, et al. Inactivating mutations of acetyltransferase genes in B-cell lymphoma. Nature 2011;471:189–95.
22. Hashwah H, Schmid CA, Kasser S, Bertram K, Stelling A, Manz MG, et al. Inactivation of CREBBP expands the germinal center B cell compartment, down-regulates MHCII expression and promotes DLBCL growth. Proc Natl Acad Sci U S A 2017;114:9701–6.
23. Horton SJ, Giotopoulos G, Yun H, Vohra S, Sheppard O, Bashford-Rogers R, et al. Early loss of Crebbp confers malignant stem cell properties on lymphoid progenitors. Nat Cell Biol 2017;19:11093–104.
24. Zhang J, Vlasevska S, Wells VA, Nataraj S, Holmes AB, Duval R, et al. The CREBBP acetyltransferase is a haploinsufficient tumor suppressor in B-cell lymphoma. Cancer Discov 2017;7:322–37.
25. Meyer SN, Scuoppo C, Vlasevska S, Bal E, Holmes AB, Holloman M, et al. Unique and shared epigenetic programs of the CREBBP and EP300 acetyltransferases in germinal center B cells reveal targetable dependencies in lymphoma. Immunity 2019;51:535–47.
26. Pastore A, Jurinovic V, Kridel R, Hoster E, Staiger AM, Szczepanowski M, et al. Integration of gene mutations in risk prognostication for patients receiving first-line immunochemotherapy for follicular lymphoma: a retrospective analysis of a prospective clinical trial and validation in a population-based registry. Lancet Oncol 2015;16:1111–22.
27. Li J, Wang J, Wang J, Nawaz Z, Liu JM, Qin J, et al. Both corepressor proteins SMRT and N-CoR exist in large protein complexes containing HDAC3. EMBO J 2000;19:4342–50.
28. Wagner FF, Lundh M, Kaya T, McCarren P, Zhang YL, Chattopadhyay S, et al. An isochemogenic set of inhibitors to define the therapeutic potential of histone deacetylases in beta-cell protection. ACS Chem Biol 2016;11:363–74.
29. Phan RT, Saito M, Basso K, Niu H, Dalla-Favera R. BCL6 interacts with the transcription factor Miz-1 to suppress the cyclin-dependent kinase inhibitor p21 and cell cycle arrest in germinal center B cells. Nat Immunol 2005;6:1054–60.
30. Tian YF, Ahn H, Schneider RS, Yang SN, Roman-Gonzalez L, Melnick AM, et al. Integrin-specific hydrogels as adaptable tumor organoids for malignant B and T cells. Biomaterials 2015;73:110–9.
31. Fujita N, Jaye DL, Geigerman C, Akyildiz A, Mooney MR, Boss JM, et al. MTA3 and the Mi-2/NuRD complex regulate cell fate during B lymphocyte differentiation. Cell 2004;119:75–86.
32. Huang C, Gonzalez DG, Cote CM, Jiang Y, Hatzi K, Teater M, et al. The BCL6 RD2 domain governs commitment of activated B cells to form germinal centers. Cell Rep 2014;8:1497–508.
33. Wilting RH, Yanover E, Heideman MR, Jacobs H, Horner J, van der Torre J, et al. Overlapping functions of Hdac1 and Hdac2 in cell cycle regulation and haematopoiesis. EMBO J 2010;29:2586–97.
34. Green MR, Monti S, Rodig SJ, Juszczynski P, Currie T, O'Donnell E, et al. Integrative analysis reveals selective 9p24.1 amplification, increased PD-1 ligand expression, and further induction via JAK2 in nodular sclerosing Hodgkin lymphoma and primary mediastinal large B-cell lymphoma. Blood 2010;116:3268–77.
35. Ansell SM, Lesokhin AM, Borrello I, Halwani A, Scott EC, Gutierrez M, et al. PD-1 blockade with nivolumab in relapsed or refractory Hodgkin's lymphoma. N Engl J Med 2015;372:311–9.
36. Xu W, Fukuyama T, Ney PA, Wang D, Rehg J, Boyd K, et al. Global transcriptional coactivators CREB-binding protein and p300 are highly essential collectively but not individually in peripheral B cells. Blood 2006;107:4407–16.
37. Beguelin W, Rivas MA, Calvo Fernández MT, Teater M, Purwada A, Redmond D, et al. EZH2 enables germinal centre formation through epigenetic silencing of CDKN1A and an Rb-E2F1 feedback loop. Nat Commun 2017;8:877.
38. Valls E, Lobry C, Geng H, Wang L, Cardenas M, Rivas M, et al. BCL6 antagonizes NOTCH2 to maintain survival of human follicular lymphoma cells. Cancer Discov 2017;7:506–21.
39. Cardenas MG, Yu W, Beguelin W, Teater MR, Geng H, Goldstein RL, et al. Rationally designed BCL6 inhibitors target activated B cell diffuse large B cell lymphoma. J Clin Invest 2016;126:3351–62.
40. Shankaran V, Ikeda H, Bruce AT, White JM, Swanson PE, Old LJ, et al. IFNgamma and lymphocytes prevent primary tumour development and shape tumour immunogenicity. Nature 2001;410:1107–11.
41. Minn AJ, Wherry EJ. Combination cancer therapies with immune checkpoint blockade: convergence on interferon signaling. Cell 2016;165:272–5.
42. Ogura M, Ando K, Suzuki T, Ishizawa K, Oh SY, Itoh K, et al. A multicentre phase II study of vorinostat in patients with relapsed or refractory indolent B-cell non-Hodgkin lymphoma and mantle cell lymphoma. Br J Haematol 2014;165:768–76.
43. Crump M, Coiffier B, Jacobsen ED, Sun L, Ricker JL, Xie H, et al. Phase II trial of oral vorinostat (suberoylanilide hydroxamic acid) in relapsed diffuse large-B-cell lymphoma. Ann Oncol 2008;19:964–9.
44. Zaidi MR, Merlino G. The two faces of interferon-gamma in cancer. Clin Cancer Res 2011;17:6118–24.
45. Peng C, Hu Q, Yang F, Zhang H, Li F, Huang C, et al. BCL6-mediated silencing of PD-1 ligands in germinal center B cells maintains follicular T cell population. J Immunol 2019;202:704–13.
46. Ran FA, Hsu PD, Wright J, Agarwala V, Scott DA, Zhang F, et al. Genome engineering using the CRISPR-Cas9 system. Nat Protoc 2013;8:2281–308.
47. Townsend EC, Murakami MA, Christodoulou A, Christie AL, Köster J, DeSouza TA, et al. The public repository of xenografts enables discovery and randomized phase II-like trials in mice. Cancer Cell 2016;29:574–86.
48. Purwada A, Jaiswal MK, Ahn H, Nojima T, Kitamura D, Gaharwar AK, et al. Ex vivo engineered immune organoids for controlled germinal center reactions. Biomaterials 2015;63:24–34.

Downloaded from http://aacrjournals.org/cancerdiscovery/article-pdf/10/3/440/1813368/440.pdf by guest on 27 August 2022